

Next-to-next-to-leading power corrections to unpolarized Semi-Inclusive Deep Inelastic Scattering

Ian Balitsky^{a,c} Alexei Prokudin^{b,c}

^a*Department of Physics, Old Dominion University, Norfolk, VA 23529, USA*

^b*Division of Science, Penn State University Berks, Reading, Pennsylvania 19610, USA*

^c*Jefferson Lab, Newport News, VA 23606, USA*

E-mail: balitsky@jlab.org, prokudin@jlab.org

ABSTRACT: Semi-Inclusive Deep Inelastic Scattering (SIDIS) is a key tool for exploring the three-dimensional structure of the nucleon through Transverse Momentum Dependent parton distributions and fragmentation functions. While leading-power contributions to the SIDIS cross-section are well established, next-to-leading (NLP) of order $1/Q$ and next-to-next-to-leading power (NNLP) corrections of order $1/Q^2$ to the hadronic tensor have only recently begun to be systematically investigated. These corrections are essential for the reliable phenomenology and interpretation of modern high-precision data. In recent papers by one of the authors, NNLP corrections to Drell-Yan process were derived using rapidity factorization formalism. In the present work we extend this approach to SIDIS and obtain analytic expressions for the unpolarized structure functions. We derive NNLP corrections that include convolutions of unpolarized distributions, f_1 , with unpolarized fragmentation functions, D_1 , and Boer-Mulders functions, h_1^\perp , with Collins fragmentation functions, H_1^\perp . We compare our results with previous formulations, provide numerical studies, confront our predictions with HERMES and COMPASS measurements, and present predictions for future experiments at Jefferson Lab and the Electron-Ion Collider.

Contents

1	Introduction	1
2	Semi-Inclusive Deep Inelastic Scattering process	3
2.1	Kinematics	3
2.2	The hadronic tensor	6
3	Structure functions	11
4	Numerical estimates and comparisons	13
4.1	$F_{UU,T}$ structure function	14
4.2	$F_{UU,L}$ structure function	16
4.3	$F_{UU}^{\cos \phi_h}$ structure function	19
4.4	$F_{UU}^{\cos 2\phi_h}$ structure function	21
4.5	Study of relations Eq. (3.19)	24
5	Conclusions and outlook	25
A	Conversions	26
B	Structure functions from Refs. [1–3]	26

1 Introduction

Semi-Inclusive Deep Inelastic Scattering is one of the most studies processes at various experimental facilities, such as HERMES [4] (DESY), COMPASS [5] (CERN), Jefferson Lab [6] and the future Electron-Ion Collider [7]. In this process a lepton with momentum l scatters off a nucleon or a nucleus with momentum P and the target is destroyed producing hadrons one of which is detected, P_h along side with the scattered lepton that has momentum l' . When the transverse momentum of the produced hadron is comparable to the virtuality of the exchanged photon, $Q^2 = -q^2 = -(l-l')^2$, or the transverse momentum $P_{h\perp}$ is integrated, the collinear QCD factorization [8] is applicable and one describes the process with collinear parton distribution and fragmentation functions that depend on the Bjorken x and z_h respectively. When the transverse momentum is small enough, $P_{h\perp}/z_h \ll Q$, the Transverse Momentum Dependent factorization is valid. The cross section is described in terms of the Transverse Momentum Dependent distribution and fragmentation functions [9], collectively called TMDs, which encode the three-dimensional (3D) structure of the nucleon.

In recent years the 3D nucleon structure attracted a lot of interest in experimental and theoretical communities, see Ref. [9] for the review. The SIDIS cross section is proportional to the convolution of the leptonic and hadronic tensors. In pioneering works by Mulders and Tangerman [1] and Kotzinian [10], the leading power and next-to-leading power $\sim 1/Q$, were calculated for the hadronic tensor that allowed to give clear interpretation of the experimental data and led to a successful phenomenological studies of both polarized and unpolarized SIDIS. This pioneering works were followed by a thorough investigation [8] of the factorization theorems that led to a good understanding of the scale dependence of TMDs. Recently phenomenology of TMDs is performed

with TMD evolution [8]. We refer the reader to Chapter 10 of TMD handbook [9] for further introduction to the sub-leading contributions in SIDIS and Drell-Yan.

Until a few years back, the next-to-next-to-leading power corrections $\sim 1/Q^2$ to the hadronic tensor of SIDIS were unknown. These corrections are potentially very important given high precision of the existing and future experimental data. Moreover, some of the structure functions, for example $F_{UU,L}$ that encode the longitudinally polarized virtual photon, were neglected as they include neither leading nor next-to-leading power contributions. Structure function $F_{UU,L}$ is studied [11] at Jefferson Lab and therefore it is timely to investigate the next-to-leading contributions in SIDIS. In addition, NLP corrections can help better understand the 3D structure of the nucleon. In unpolarized scattering, they may be important for understanding of the observed multiplicities, $\cos \phi_h$ ¹, and $\cos 2\phi_h$ modulations of the cross sections. This in turn will be important for the understanding of spin asymmetries and extractions of polarized TMDs, for instance the transversity function [12] that is the only source of the direct information about the tensor charge of the nucleon.

Recently NLP corrections were investigated by Ebert, Gao, and Stewart in Ref. [13], by Gamberg et al in Ref [?], and by Rodini and Vladimirov in Ref. [14]. TMD operator product expansion at NLP was studied by Vladimirov, Moos, Scimemi in Ref. [15]. Kinematic power corrections to TMD factorization were studied by Vladimirov in Ref. [16], and by Piloñeta and Vladimirov in Ref. [17], and kinematic next-to-next-to-leading power corrections were derived to hadronic tensor in SIDIS. Jet production in SIDIS at next-to-leading power was investigated in Ref. [18].

In this paper we will extend rapidity factorization formalism [19], of one of the authors, which was used for Drell-Yan in Refs. [20, 21] and apply it to Semi-Inclusive Deep Inelastic Scattering. We will derive $\sim 1/Q^2$ corrections to the hadronic tensor that include convolutions of unpolarized distributions, f_1 , with unpolarized fragmentation functions, D_1 and Boer-Mulders functions [22], h_1^\perp , with Collins fragmentation functions [23], H_1^\perp and obtain formulas for the unpolarized structure functions in Semi-Inclusive Deep Inelastic Scattering: $F_{UU,T}$, $F_{UU,L}$, $F_{UU}^{\cos \phi_h}$, and $F_{UU}^{\cos 2\phi_h}$. We will compare our results to the existing formulas from [13, 17] and other papers and present numerical estimates and comparisons to the experimental data from HERMES and COMPASS. We will also provide estimates for future measurements of the ratio $F_{UU,L}/F_{UU,T}$ at Jefferson Lab and the future Electron-Ion Collider.

The paper is organized as follows: in Sec. 2.1 we will introduce kinematics and our notations for SIDIS, in Sec. 2.2 we will extend the rapidity factorization formalism formalism [21] to SIDIS and derive the SIDIS hadron tensor including next-to-next-to-leading power corrections $\sim 1/Q^2$. In Sec. 3 we will derive expressions for $F_{UU,T}$, $F_{UU,L}$, $F_{UU}^{\cos \phi_h}$, and $F_{UU}^{\cos 2\phi_h}$ structure functions. In Sec. 4 we will provide numerical estimates, compare to the experimental data, and compare our formulas to the existing results. In particular, we will investigate $F_{UU,T}$ due to transversely polarized photons in Sec. 4.1 and compare our results to the experimental data. We will explore $F_{UU,L}$ due to the longitudinal photon polarization in Sec. 4.1 and give predictions for R_{SIDIS} to be measured at Jefferson Lab and the EIC. In Sec. 4.3 we will study the subleading $\sim 1/Q$ structure function $F_{UU}^{\cos \phi_h}$ and the corresponding asymmetry, and in Sec. 4.4 we will investigate $F_{UU}^{\cos 2\phi_h}$ structure function that has the leading contribution from convolution of Boer-Mulders [22] and Collins [23] functions. We conclude and discuss future directions in Sec. 5.

¹ ϕ_h is the azimuthal angle of the produced hadron with respect to the lepton scattering plane.

2 Semi-Inclusive Deep Inelastic Scattering process

2.1 Kinematics

In this section we will define the kinematics of the process and introduce our notations. The Semi-Inclusive Deep Inelastic Scattering process (SIDIS)

$$\ell(l) + p(P) \rightarrow \ell(l') + h(P_h) + X, \quad (2.1)$$

in the single-photon exchange approximation is sketched in Fig. 1. Here, l and P are the momenta of the incoming lepton ℓ and the nucleon p ; l' and P_h are the momenta of the outgoing lepton ℓ and of the detected produced hadron h . The center-of-mass energy of the process is $s = (l + P)^2$, the virtual-photon momentum $q = l - l'$ defines the z -axis of the Trento $\gamma^* P$ frame [24], its virtuality is $Q^2 = -q^2$. Vectors l' and l define the lepton plane and l' points in the direction of the x -axis from which azimuthal angles are counted. The produced hadron h has the momentum P_h and its transverse momentum is $P_{h\perp}$. Vectors q and P_h define the hadron plane. The fully differential cross-section at $Q^2 \ll M_Z^2$ reads [1, 2, 10]:

$$d\sigma = \frac{\alpha_{em}^2}{(l \cdot P) Q^4} L_{\mu\nu} W^{\mu\nu} \frac{d^3 l'}{2E_{l'}} \frac{d^3 P}{2E_P} \quad (2.2)$$

where $L_{\mu\nu}$ is the leptonic tensor

$$L_{\mu\nu} = 2(l_\mu l'_\nu + l'_\mu l_\nu - (l \cdot l') g_{\mu\nu}) + 2i\lambda_l \epsilon^{\mu\nu\rho\sigma} l_\rho l'_\sigma, \quad (2.3)$$

where λ_l is the helicity of the lepton, and $W_{\mu\nu}$ is the hadronic tensor²

$$W_{\mu\nu}(q) \stackrel{\text{def}}{=} \frac{1}{(2\pi)^4} \sum_X \int d^4 x e^{iq \cdot x} \langle P | J_\mu(x) | P_h + X \rangle \langle P_h + X | J_\nu(0) | P \rangle. \quad (2.4)$$

The relevant kinematic variables expressed via Lorentz invariants are:

$$x = \frac{Q^2}{2P \cdot q}, \quad y = \frac{P \cdot q}{P \cdot l}, \quad z_h = \frac{P \cdot P_h}{P \cdot q}. \quad (2.5)$$

In addition to x , y , and z_h , the cross section is also differential in the azimuthal angle ϕ_h of the produced hadron, in the square of the hadron's momentum component $P_{h\perp}$, and in the azimuthal angle of the outgoing lepton l' around beam axis, $\psi \approx \phi_S$ in $Q \gg M$ limit.

In the one photon exchange approximation SIDIS process can be characterized by 18 independent structure functions [1, 2, 10]. We will consider unpolarized scattering where 4 structure functions contribute to the process [1, 2, 10]:

$$\frac{d\sigma}{dx dy dz_h d\phi_h dP_{h\perp}^2} = \sigma_0 \left[F_{UU,T} + p_1 F_{UU,L} + \cos(\phi_h) p_3 F_{UU}^{\cos \phi_h} + \cos(2\phi_h) p_1 F_{UU}^{\cos 2\phi_h} \right], \quad (2.6)$$

where

$$\sigma_0 = \frac{2\pi\alpha_{em}^2}{xyQ^2} \left(1 - y + \frac{1}{2}y^2 \right) \quad (2.7)$$

Up to corrections suppressed as $1/Q^2$, the kinematic prefactors p_i in Eq. (2.6) are given by [25]

$$p_1 = \frac{1-y}{1-y+\frac{1}{2}y^2}, \quad p_3 = \frac{(2-y)\sqrt{1-y}}{1-y+\frac{1}{2}y^2}. \quad (2.8)$$

²Here \sum_X denotes the sum over full set of “out” states and $J_\mu = \sum e_f \bar{\psi}^f \gamma_\mu \psi^f$ is the electromagnetic current. We take into account only u, d, s quarks and consider them massless.

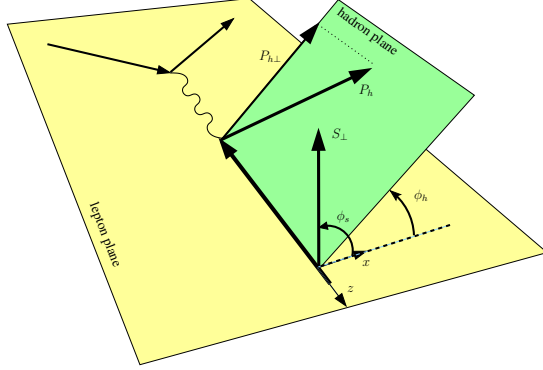


Figure 1: Kinematics of the SIDIS process $lp \rightarrow l'hX$ in the one photon exchange approximation in the Trento frame [24].

The structure functions in Eq. (2.6) implicitly depend on $x, z_h, P_{h\perp}^2$ and Q^2 . Their superscripts indicate the azimuthal dependence. The subscripts encode the beam and target polarizations. The first subscript UU denotes the unpolarized beam and the target, the second superscript refers to either longitudinal, L , or transverse, T , virtual photon polarizations.

For SIDIS process there are two distinct choices [8, 9] for frames, see Fig. 2. In hadron-hadron frame, Fig. 2 (b), one defines transverse direction relative to the incoming hadron p and produced hadron h , each of those having zero transverse momentum. In this frame all transverse directions will be labeled with a subscript “ T ”. In this frame the transverse momentum of the virtual photon q_T is non zero and is related to the transverse momentum \mathbf{k}_T of the parton in p and the fragmenting parton \mathbf{p}'_T relative to the detected hadron h .

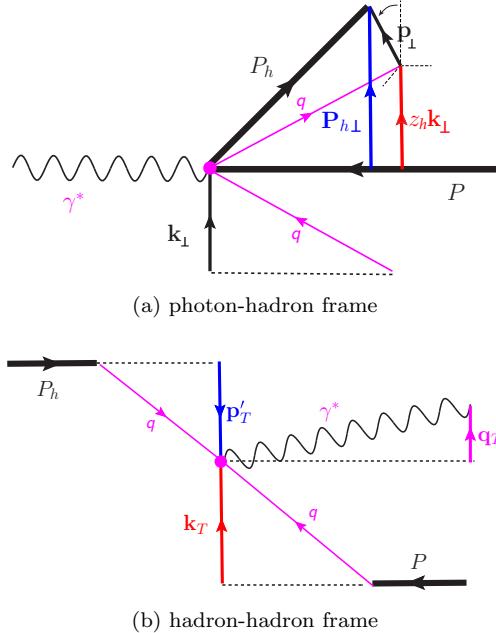


Figure 2: Illustration of the the two frames used to describe the kinematics of the SIDIS process, as discussed in the text. The figure is from Ref. [9].

Their relation in the region of validity of the TMD factorization theorem, $\mathbf{q}_T^2/Q^2 \ll 1$, reads

$$\mathbf{q}_T = -\mathbf{k}_T + \mathbf{p}'_T \quad (2.9)$$

The second choice is photon-hadron frame [9, 24], Fig. 2 (a). In this case \mathbf{q} is aligned with z axis and the incoming hadron still has the vanishing transverse momentum. In this frame all transverse directions will be labeled with a subscript “ \perp ”. The interpretation of the transverse momentum of the parton in p is the same, \mathbf{k}_\perp , however the outgoing hadron h has transverse momentum \mathbf{p}_\perp relative to the fragmenting parton and the transverse momentum of the produced hadron $P_{h\perp}$ in this frame is

$$\mathbf{P}_{h\perp} = z_h \mathbf{k}_\perp + \mathbf{p}_\perp \quad (2.10)$$

For a sufficiently large $Q^2 \gg M^2$ the two frames are related as follows

$$\mathbf{k}_\perp = \mathbf{k}_T, \mathbf{p}_\perp = -z_h \mathbf{p}'_T, \mathbf{P}_{h\perp} = -z_h \mathbf{q}_T. \quad (2.11)$$

The subtleties of the two frames and the definitions of the convolutions are discussed in Ref. [17]. In order to simplify our discussion we will work in the approximation $Q^2 \gg M^2$ where Eqs. (2.11) hold.

Structure functions in Eq. (2.6) are described in terms of convolutions of TMDs PDFs, f and TMD FFs, D , in the region where the TMD factorization is valid, and the generic structure of the convolution in our approximation reads [1, 2]

$$\begin{aligned} \mathcal{C}[\omega f D] &= x \sum_a H_{aa}(Q^2, \mu^2) \int d^2 \mathbf{k}_\perp d^2 \mathbf{p}_\perp \delta^{(2)}(z_h \mathbf{k}_\perp + \mathbf{p}_\perp - \mathbf{P}_{h\perp}) \omega f^a(x, \mathbf{k}_\perp^2) D^a(z_h, \mathbf{p}_\perp^2) \\ &= x \sum_a H_{aa}(Q^2, \mu^2) \int d^2 \mathbf{k}_\perp \omega f^a(x, \mathbf{k}_\perp^2) D^a(z_h, (\mathbf{P}_{h\perp} - z_h \mathbf{k}_\perp)^2) \end{aligned} \quad (2.12)$$

$$\begin{aligned} &= x \sum_a H_{aa}(Q^2, \mu^2) \int d^2 \mathbf{k}_T d^2 \mathbf{p}'_T \delta^{(2)}(\mathbf{k}_T - \mathbf{p}'_T + \mathbf{q}_T) \omega f^a(x, \mathbf{k}_T^2) D^a(z_h, (-z_h \mathbf{p}'_T)^2) \\ &= x \sum_a H_{aa}(Q^2, \mu^2) \int d^2 \mathbf{k}_T \omega f^a(x, \mathbf{k}_T^2) D^a(z_h, (-z_h(\mathbf{q}_T + \mathbf{k}_T))^2), \end{aligned} \quad (2.13)$$

the first two lines, Eq. (2.12), describe the convolution in photon-hadron frame, while the last two lines, Eq. (2.13), define the convolution in hadron-hadron frame. Here ω is a weight function, which in general depends on the transverse momenta of incoming and outgoing quarks in the Trento frame, \mathbf{k}_\perp , \mathbf{p}_\perp , or hadron frame \mathbf{k}_T , \mathbf{p}'_T , and $\hat{\mathbf{h}} = \mathbf{P}_{h\perp}/P_{h\perp} = -\mathbf{q}_T/q_T$, and the sum runs over all quark and anti-quark flavors $a = u, \bar{u}, d, \bar{d}$, etc. Here, the hard function³ for the SIDIS process is denoted by H_{aa} . Each TMD obeys TMD evolutions equations and depends on two scales (not shown in equations above) corresponding to the regulator for the ultra violet divergence, μ , and the regulator for the rapidity divergence, ζ , see Ref. [8, 9]. In the following, the flavor index a and the scale dependence of TMDs will be omitted in our formulas.

Notice that according to Refs. [8, 9, 26–28] the density interpretation of TMD FFs requires that they depend on \mathbf{p}_\perp^2 in photon-hadron frame or on $(-z_h \mathbf{p}'_T)^2$ in hadron-hadron frame, it is also evident in our Eqs. (2.12) and (2.13). In the following Section we will indicate this dependence explicitly.

³Notice that generally, the hard function may be off-diagonal, $H_{aa'}$, in particular at N3LL. We will consider the lowest order in which it is diagonal and trivial $H_{aa}(Q^2, Q^2) = e_a^2$.

2.2 The hadronic tensor

Information on the structure of the target is encoded in the hadronic tensor. Leading power and next-to-leading-power hadronic tensor for SIDIS was introduced by Mulders and Tangerman [1] and Kotzinian [10], and next-to-leading-power SIDIS hadronic tensor was studied by Ebert, Gao, and Stewart Ref. [13] and by Rodini and Vladimirov in Ref. [14]. Next-to-next-to-leading-power kinematic corrections were studied by Vladimirov in Ref. [16] and by Piloñeta and Vladimirov in Ref. [17].

Here we will outline how to obtain power corrections to SIDIS hadronic tensor from the corresponding results for the Drell-Yan using the rapidity factorization formalism [20, 21]. In Drell-Yan process two hadrons A and B collide and produce a detected lepton-antilepton pair

$$p(P_A) + p(P_B) \rightarrow \ell^+(l) + \ell^-(l') + X. \quad (2.14)$$

The center of mass energy is $s = (P_A + P_B)^2$. When the transverse component q_T of the $\ell^+\ell^-$ final state momentum, $q = l + l'$, is small compared to its invariant mass $Q^2 = q^2$, i.e. $q_T^2 \ll Q^2$, TMD factorization theorem is valid and the hadronic tensor contains TMD PDFs of hadrons A and B . For Drell-Yan it is natural to use the hadron directions as reference directions and therefore one discusses the quark transverse momentum as relative to its parent hadron.

We will call hadron A projectile and hadron B target. In the methodology of Ref. [19] quark and gluon fields of the target and projectile are separated in three sectors: “projectile” fields with small components along the target, “target” fields with small components along the projectile, and “central” fields which are neither projectile no target ones. In order to obtain the TMD factorization, one “freezes” the projectile and target fields and integrates over the central fields. The result of the integration is a series of diagrams in the background of projectile and target fields. At the tree level, the sum of such diagrams describes a solution of QCD classical equations with sources being projectile and target fields. The general solution known as the scattering of two “color glass condensates,” is not known at present. However, if $q_T^2/Q^2 \ll 1$, one can use this ratio as an expansion parameter to obtain the solution as a series of projectile and target TMD operators suppressed by powers of Q^2 . At this step, there is no difference between the DY and SIDIS cases. The difference comes after integration over the projectile and target fields yielding the TMD matrix elements. The target matrix elements for SIDIS are the same as in DY with the exception of a different direction of the corresponding gauge links out to $+\infty$ instead of $-\infty$ for the DY case. As to the projectile matrix elements, the TMD PDFs of the projectile should be replaced by TMD fragmentation functions (TMD FFs). In order to be consistent with the notations for the previous Section, we will modify conventions of Refs. [20, 21]: $\perp \rightarrow T$, $x \rightarrow b$.

We will use Sudakov variables α and β to parametrize $q = \alpha p_1 + \beta p_2 + q_T$ where p_1 and p_2 are light-like vectors, in Drell-Yan, $P_A = p_1 + (M_A^2/s) p_2$ and $P_B = p_2 + (M_B^2/s) p_1$. We neglect hadron masses, i.e. $P_A^2 = P_B^2 = 0$, and thus $p_1^\mu = P_A^\mu$ and $p_2^\mu = P_B^\mu$. In Semi-Inclusive Deep Inelastic Scattering, $p_1^\mu = P_h^\mu$ and $p_2^\mu = P^\mu$. We use the following notation for two vector products: $(a, b)_T \equiv \mathbf{a}_T \cdot \mathbf{b}_T$. We define $\varsigma \equiv 2(p_1 \cdot p_2)$ so that in DY $\varsigma = 2(P_A \cdot P_B) = s$ while in SIDIS $\varsigma = 2(P \cdot P_h) = Q^2 z_h/x$. For Drell-Yan, $\alpha \equiv x_1$ and $\beta \equiv x_2$ and one obtains the standard relation $Q^2 = x_1 x_2 s - q_T^2 > 0$. In SIDIS, $\alpha = 1/z_h$, $\beta = -x(1 - q_T^2/Q^2)$ and one has $q^2 \equiv -Q^2 < 0$.

The metric tensor can be written in terms of longitudinal and transverse parts as follows

$$g^{\mu\nu} = g_{\parallel}^{\mu\nu} + g_T^{\mu\nu} = \frac{p_1^\mu p_2^\nu + p_2^\nu p_1^\mu}{(p_1 \cdot p_2)} + g_T^{\mu\nu}, \quad (2.15)$$

$$g_{\parallel}^{\mu\nu\text{DY}} = \frac{2}{s} (p_1^\mu p_2^\nu + p_2^\nu p_1^\mu), \quad (2.16)$$

$$g_{\parallel}^{\mu\nu\text{SIDIS}} = \frac{2x}{z_h Q^2} (p_1^\mu p_2^\nu + p_2^\nu p_1^\mu). \quad (2.17)$$

We will use the transverse tensors $g_T^{\mu\nu}$ and $\epsilon_T^{\mu\nu}$, whose only nonzero components are $g_T^{11} = g_T^{22} = 1$ and $\epsilon_T^{12} = -\epsilon_T^{21} = 1$.

TMDs are defined by the following quark-quark correlator, see e.g. Ref. [2, 9],

$$\begin{aligned}\Phi_{ij}(x, \mathbf{k}_T) &= \int \frac{db^- d^2 b_T}{8\pi^3} e^{-ixP^+ b^- + i(k, b)_T} \langle P | \bar{\psi}_j(b) [b, \infty] [\infty, 0] \psi_i(0) | P \rangle \\ &= \frac{1}{2} \left[f_1(x, \mathbf{k}_T) \not{n}_+ + i h_1^\perp \frac{[\not{k}_T, \not{n}_+]}{2M} \right]_{ij} + \frac{M}{2P^+} \left[e + f^\perp \frac{\not{k}_T}{M} - \frac{g^\perp \gamma_5}{M} \epsilon_T^{\rho\sigma} \gamma_\rho k_{T\sigma} + \frac{i}{2} h [\not{n}_+, \not{n}_-] \right]_{ij} \quad (2.18)\end{aligned}$$

where we include only the functions related to the unpolarized scattering that we study in this paper and indicate the functional dependence only for the unpolarized TMD, f_1 , for brevity. In Eq. (2.18) two light-like vectors n_+ and n_- are used, such that for any four vector a one has $a^+ = a \cdot n^-, a^- = a \cdot n^+$ and $a_T \cdot n^+ = a_T \cdot n^- = 0$. They are related to our Sudakov vectors as follows

$$n_+^\mu \equiv \frac{p_2^\mu}{\sqrt{\varsigma/2}}, \quad n_-^\mu \equiv \frac{p_1^\mu}{\sqrt{\varsigma/2}}. \quad (2.19)$$

Notice that in the frame we consider for SIDIS

$$P^+ = P \cdot n_- = \sqrt{\varsigma/2}, \quad P_h^- = P_h \cdot n_+ = \sqrt{\varsigma/2}. \quad (2.20)$$

The leading twist unpolarized TMD is projected from the correlator as

$$f_1(x, \mathbf{k}_T^2) = \frac{1}{2} \text{Tr} \left[\gamma^+ \Phi(x, \mathbf{k}_T) \right] \quad (2.21)$$

while the subleading TMDs are obtained by projecting with $\mathbb{1}$ and γ^i .

The correlator for the fragmentation functions reads

$$\begin{aligned}\Delta_{ij}(z_h, \mathbf{k}_T) &= \frac{1}{2z_h N_c} \int \frac{db^+ d^2 b_T}{8\pi^3} e^{iP^-/z_h b^+ - i(k, b)_T} \sum_X \langle 0 | \psi_i(b) | P_h + X \rangle \langle P_h + X | \bar{\psi}_j(0) | 0 \rangle \\ &= \frac{1}{2} \left[D_1(z_h, z_h^2 \mathbf{k}_T^2) \not{n}_- + i H_1^\perp \frac{[\not{k}_T, \not{n}_-]}{2m_N} \right] + \frac{m_N}{2P^-} \left[E + F^\perp \frac{\not{k}_T}{m_N} + \frac{G^\perp \gamma_5}{m_N} \epsilon_T^{\rho\sigma} \gamma_\rho k_{T\sigma} + \frac{i}{2} H [\not{n}_-, \not{n}_+] \right] \quad (2.22)\end{aligned}$$

where functional dependence is indicated only for D_1 for brevity. In SIDIS the produced hadron moves fast in the “ $-$ ” light-cone direction, and the twist-2 TMD FF is projected out as

$$D_1(z_h, z_h^2 \mathbf{k}_T^2) = \frac{1}{2} \text{Tr} [\gamma^- \Delta(z_h, \mathbf{k}_T)] \quad (2.23)$$

while subleading TMD FFs are obtained by projecting with $\mathbb{1}$ and γ^i .

For the DY process the large- N_c power corrections up to $1/Q^2$ were obtained in Ref. [21] by using QCD equations to convert quark-antiquark-gluon ($\bar{q}Fq$) TMDs to quark-antiquark ($\bar{q}q$) TMDs. For example, QCD Dirac equation of motion (EOM) equation

$$\bar{\psi}(b) \mathcal{A}_T(b) = i \partial_i \bar{\psi}(b) \gamma^i + i \sqrt{\frac{2}{\varsigma}} \partial_+ \bar{\psi}(b) \not{p}_1 + i \sqrt{\frac{2}{\varsigma}} \bar{\psi}(b) \not{D}_+ \not{p}_2 \quad (2.24)$$

leads to

$$\begin{aligned}&\frac{\sqrt{2/\varsigma}}{16\pi^3} \int db^+ d^2 b_T e^{-i\alpha \sqrt{\varsigma/2} b^+ + i(q-k, b)_T} \langle p_A | \bar{\psi}(b^+, \mathbf{b}_T) \mathcal{A}(b^+, \mathbf{b}_T) \not{p}_B \gamma_i \psi(0) | p_A \rangle \\ &= (q-k)_i \{ f_1(\alpha, (\mathbf{q}_T - \mathbf{k}_T)^2) - \alpha [f^\perp(\alpha, (\mathbf{q}_T - \mathbf{k}_T)^2) + ig^\perp(\alpha, (\mathbf{q}_T - \mathbf{k}_T)^2)] \} \quad (2.25)\end{aligned}$$

and

$$\begin{aligned} & \frac{\sqrt{2/\zeta}}{16\pi^3} \int db^+ d^2\mathbf{b}_T e^{-i\alpha\sqrt{\zeta/2}b^+ + i(q-k,b)_T} \langle p_A | \bar{\psi}(b^+, \mathbf{b}_T) \mathcal{A}(b^+, \mathbf{b}_T) \not{p}_B \psi(0) | p_A \rangle \\ &= \left\{ -i \frac{(q-k)_T^2}{M} h_1^\perp(\alpha, (\mathbf{q}_T - \mathbf{k}_T)^2) - M\alpha [e(\alpha, (\mathbf{q}_T - \mathbf{k}_T)^2) + ih(\alpha, (\mathbf{q}_T - \mathbf{k}_T)^2)] \right\} \quad (2.26) \end{aligned}$$

where the real part in brackets in the RHS of Eq. (2.25) is usually denoted as $-x\tilde{f}^\perp$ and imaginary part in Eq. (2.26) is denoted as $x\tilde{h}$. Those tilde terms are neglected in WW approximations. The terms such as these are important for the restoration of the EM gauge-invariance, see Ref. [20]. A nontrivial observation made in Ref. [20] for the Drell-Yan process is that, when all contributions originating from $\bar{\psi}(x)\mathcal{A}(x)$ and $\mathcal{A}(0)\psi(0)$ are properly combined, one obtains an electromagnetic gauge-invariant contribution involving the functions f_1 and h_1^\perp . We refer to this result as the gauge completion of the leading-twist contribution. In contrast, for the terms proportional to f^\perp and h , as discussed in Ref. [20], achieving gauge invariance requires corrections of order $1/Q^3$. It is therefore natural to examine the assumption that the gauge completion of leading-twist functions is numerically more important than that of higher-twist functions. A comparison [29] with experimental data on the Z -boson angular coefficients indicates that this approximation is indeed reasonable.

The EOM equations of Eqs. (2.24,2.26) type are the same for the case of SIDIS. However, the Fourier transform of fragmentation functions defined in Eq. (2.22) is somewhat different, so we get instead of Eq. (2.25)

$$\begin{aligned} & \frac{\sqrt{2/\zeta}}{16\pi^3} \frac{\alpha}{2N_c} \int db^+ d^2\mathbf{b}_T e^{i\alpha\sqrt{\zeta/2}b^+ - i(q+k,b)_T} \sum_X \langle 0 | \bar{\psi}(b^+, \mathbf{b}_T) \mathcal{A}(b^+, \mathbf{b}_T) | p_A + X \rangle \langle p_A + X | \not{p}_B \gamma_i \psi(0) | N \rangle \\ &= -(q+k)_i \left(\bar{D}_1 \left(\frac{1}{\alpha}, \frac{1}{\alpha^2} (\mathbf{q}_T + \mathbf{k}_T)^2 \right) - \alpha [\bar{F}^\perp - i\bar{G}^\perp] \right) \quad (2.27) \end{aligned}$$

and

$$\begin{aligned} & \frac{\sqrt{2/\zeta}}{16\pi^3} \frac{\alpha}{2N_c} \int db^+ d^2\mathbf{b}_T e^{i\alpha\sqrt{\zeta/2}b^+ - i(q+k,b)_T} \sum_X \langle 0 | \bar{\psi}(b^+, \mathbf{b}_T) \mathcal{A}(b^+, \mathbf{b}_T) | p_A + X \rangle \langle p_A + X | \not{p}_B \psi(0) | N \rangle \\ &= \left[i \frac{(q+k)_T^2}{m_h} \bar{H}_1^\perp \left(\frac{1}{\alpha}, \frac{1}{\alpha^2} (\mathbf{q}_T + \mathbf{k}_T)^2 \right) + \alpha m_h (\bar{E} + i\bar{H}) \right] \quad (2.28) \end{aligned}$$

Here for brevity we indicate the functional dependence only for D_1 and H_1^\perp .

If one considers the analytic continuation of ${}^{\text{DY}}W_{\mu\nu}(-q)$:

$$\begin{aligned} & \frac{\sqrt{2/\zeta}}{16\pi^3} \int db^- d^2\mathbf{b}_T e^{i\alpha\sqrt{\zeta/2}b^- - i(q+k,b)_T} \langle p_A | \bar{\psi}(b^-, \mathbf{b}_T) \mathcal{A}(b^-, \mathbf{b}_T) \not{p}_B \gamma_i \psi(0) | p_A \rangle \quad (2.29) \\ &= -(q+k)_i (f_1(-\alpha, (-\mathbf{q}_T - \mathbf{k}_T)^2) + \alpha [f^\perp(-\alpha, (-\mathbf{q}_T - \mathbf{k}_T)^2) + ig^\perp(-\alpha, (-\mathbf{q}_T - \mathbf{k}_T)^2)]) , \end{aligned}$$

the Fourier transform has the same structure as one in Eq. (2.27). Similarly, analytic continuation of Eq. (2.26) gives

$$\begin{aligned} & \frac{\sqrt{2/\zeta}}{16\pi^3} \int db^+ d^2\mathbf{b}_T e^{i\alpha\sqrt{\zeta/2}b^+ - i(q+k,x)_\perp} \langle p_A | \bar{\psi}(b^+, \mathbf{b}_T) \mathcal{A}(b^+, \mathbf{b}_T) \not{p}_B \psi(0) | p_A \rangle \quad (2.30) \\ &= \left[-i \frac{(q+k)_T^2}{M} h_1^\perp(-\alpha, (-\mathbf{q}_T - \mathbf{k}_T)^2) + \alpha M [e(-\alpha, (-\mathbf{q}_T - \mathbf{k}_T)^2) + ih(-\alpha, (-\mathbf{q}_T - \mathbf{k}_T)^2)] \right] \end{aligned}$$

which has the same structure as Eq. (2.28).

In general, it can be demonstrated that one can use for SIDIS literally the same formulas as in the DY case using the following procedure: one constructs SIDIS hadronic tensor from Ref. [21] by the analytical continuation of the DY hadronic tensor to negative $q \rightarrow -q$, replacing $M \rightarrow m_h$, and by replacing TMD PDFs of the projectile by TMD FFs according to the following rules:

$$f_1(-\alpha, (-\mathbf{k}_T)^2) \rightarrow \bar{D}_1\left(\frac{1}{\alpha}, \frac{\mathbf{k}_T^2}{\alpha^2}\right) \frac{2N_c}{\alpha}, \quad f^\perp(-\alpha, (-\mathbf{k}_T)^2) \rightarrow -\bar{F}^\perp\left(\frac{1}{\alpha}, \frac{\mathbf{k}_T^2}{\alpha^2}\right) \frac{2N_c}{\alpha},$$

$$g^\perp(-\alpha, (-\mathbf{k}_T)^2) \rightarrow -\bar{G}^\perp\left(\frac{1}{\alpha}, \frac{\mathbf{k}_T^2}{\alpha^2}\right) \frac{2N_c}{\alpha}, \quad (2.31)$$

$$\bar{f}_1(-\alpha, (-\mathbf{k}_T)^2) \rightarrow D_1\left(\frac{1}{\alpha}, \frac{\mathbf{k}_T^2}{\alpha^2}\right) \frac{2N_c}{\alpha}, \quad \bar{f}^\perp(-\alpha, (-\mathbf{k}_T)^2) \rightarrow -F^\perp\left(\frac{1}{\alpha}, \frac{\mathbf{k}_T^2}{\alpha^2}\right) \frac{2N_c}{\alpha},$$

$$\bar{g}^\perp(-\alpha, (-\mathbf{k}_T)^2) \rightarrow -G^\perp\left(\frac{1}{\alpha}, \frac{\mathbf{k}_T^2}{\alpha^2}\right) \frac{2N_c}{\alpha}. \quad (2.32)$$

and

$$\bar{h}_1^\perp(-\alpha, (-\mathbf{k}_T)^2) \rightarrow -H_1^\perp\left(\frac{1}{\alpha}, \frac{\mathbf{k}_T^2}{\alpha^2}\right) \frac{2N_c}{\alpha}, \quad \bar{h}(-\alpha, (-\mathbf{k}_T)^2) \rightarrow H^\perp\left(\frac{1}{\alpha}, \frac{\mathbf{k}_T^2}{\alpha^2}\right) \frac{2N_c}{\alpha},$$

$$h_3(-\alpha, (-\mathbf{k}_T)^2) \rightarrow -\bar{H}_3\left(\frac{1}{\alpha}, \frac{\mathbf{k}_T^2}{\alpha^2}\right) \frac{2N_c}{\alpha}, \quad (2.33)$$

$$h_1^\perp(-\alpha, (-\mathbf{k}_T)^2) \rightarrow -\bar{H}_1^\perp\left(\frac{1}{\alpha}, \frac{\mathbf{k}_T^2}{\alpha^2}\right) \frac{2N_c}{\alpha}, \quad \bar{h}(-\alpha, (-\mathbf{k}_T)^2) \rightarrow H^\perp\left(\frac{1}{\alpha}, \frac{\mathbf{k}_T^2}{\alpha^2}\right) \frac{2N_c}{\alpha},$$

$$\bar{h}_3(-\alpha, (-\mathbf{k}_T)^2) \rightarrow -H_3\left(\frac{1}{\alpha}, \frac{\mathbf{k}_T^2}{\alpha^2}\right) \frac{2N_c}{\alpha}, \quad (2.34)$$

and

$$f_3(-\alpha, (-\mathbf{k}_T)^2) \rightarrow \bar{F}_3\left(\frac{1}{\alpha}, \frac{\mathbf{k}_T^2}{\alpha^2}\right) \frac{2N_c}{\alpha}, \quad e(-\alpha, (-\mathbf{k}_T)^2)_\perp \rightarrow -\bar{E}\left(\frac{1}{\alpha}, \frac{\mathbf{k}_T^2}{\alpha^2}\right) \frac{2N_c}{\alpha},$$

$$h_3(-\alpha, (-\mathbf{k}_T)^2) \rightarrow -\bar{H}_3\left(\frac{1}{\alpha}, \frac{\mathbf{k}_T^2}{\alpha^2}\right) \frac{2N_c}{\alpha}, \quad (2.35)$$

$$\bar{f}_3(-\alpha, (-\mathbf{k}_T)^2) \rightarrow F_3\left(\frac{1}{\alpha}, \frac{\mathbf{k}_T^2}{\alpha^2}\right) \frac{2N_c}{\alpha}, \quad \bar{e}(-\alpha, (-\mathbf{k}_T)^2)_\perp \rightarrow -E\left(\frac{1}{\alpha}, \frac{\mathbf{k}_T^2}{\alpha^2}\right) \frac{2N_c}{\alpha},$$

$$\bar{h}_3(-\alpha, (-\mathbf{k}_T)^2) \rightarrow -H_3\left(\frac{1}{\alpha}, \frac{\mathbf{k}_T^2}{\alpha^2}\right) \frac{2N_c}{\alpha}. \quad (2.36)$$

The complete result for $\mathcal{O}(1/Q^2)$ and leading- N_c power corrections to DY hadronic tensor reads [21]

$${}^{\text{DY}}W_{\mu\nu}(q) = \sum_a e_a^2 [W_{\mu\nu}^1(q) + W_{\mu\nu}^2(q) + W_{\mu\nu}^3(q)] + \mathcal{O}\left(\frac{1}{Q^3}\right) + \mathcal{O}\left(\frac{1}{N_c^2}\right) \quad (2.37)$$

The first, EM-gauge invariant part is a “gauge completion” of the leading-twist result:

$${}^{\text{DY}}W_{\mu\nu}^1(q) = \frac{1}{N_c} \int d^2\mathbf{k}_T \left({}^{\text{DY}}\mathcal{W}_{\mu\nu}^F(q, \mathbf{k}_T) [f_1(\alpha, \mathbf{q}_T - \mathbf{k}_T) \bar{f}_1(\beta, \mathbf{k}_T) + f_1 \leftrightarrow \bar{f}_1] \right. \\ \left. + {}^{\text{DY}}\mathcal{W}_{\mu\nu}^H(q, \mathbf{k}_T) \{h_1^\perp(\alpha, \mathbf{q}_T - \mathbf{k}_T) \bar{h}_1^\perp(\beta, \mathbf{k}_T) + h_1^\perp \leftrightarrow \bar{h}_1^\perp\} \right) \quad (2.38)$$

where the transverse structures ${}^{\text{DY}}\mathcal{W}_{\mu\nu}^F(q, \mathbf{k}_T)$ and ${}^{\text{DY}}\mathcal{W}_{\mu\nu}^H(q, \mathbf{k}_T)$ are given by Eqs. (7.3) and (7.4) from Ref. [21] and the flavor index a is implicit for all TMD functions. The second term, containing quark-antiquark TMDs of the sub-leading twist, is also EM gauge invariant while $W_{\mu\nu}^3(q)$ is made of quark-quark-gluon TMDs which cannot be reduced to quark-antiquark TMDs by EOMs. These

$\bar{q}Fq$ TMDs in $W_{\mu\nu}^3(q)$ cannot be reduced to the $\bar{q}q$ so these TMDs should be parametrized similarly to the DY case.

The number of different TMDs is about 30, so it would be very useful to understand which ones are the most important numerically. In Refs. [29, 30] the angular distributions of Z -boson DY production were calculated using the assumption that the contribution of the function f_1 is the most significant one. The estimations from Ref. [29] agree well with the LHC data: the coefficients A_0 and A_2 agree with $1/N_c \sim 30\%$ accuracy while other angular coefficients, that are zero under naive estimations, are experimentally found to be an order of magnitude smaller than A_0 and A_2 .

In this paper we would like to test similar approximations. We will take into account the leading-twist distributions f_1, D_1 and h_1^\perp, H_1^\perp and their “gauge completions.” That is in Eq. (2.29) only f_1 remains. In this approximation, SIDIS hadronic tensor takes the form

$$W_{\mu\nu}^1(q) = 2z_h \int d^2\mathbf{k}_T (\mathcal{W}_{\mu\nu}^F(q, \mathbf{k}_T) \{D_1 f_1 + \bar{D}_1 \bar{f}_1\} - \mathcal{W}_{\mu\nu}^H(q, \mathbf{k}_T) \kappa \{H_1^\perp h_1^\perp + \bar{H}_1^\perp \bar{h}_1^\perp\}) \quad (2.39)$$

where $\kappa = -1$ for SIDIS and $\kappa = 1$ for Drell-Yan, such that κh_1^\perp always corresponds to Boer-Mulders function in a particular process:

$$h_1^{\perp(\text{DY})} = h_1^\perp \text{ and } h_1^{\perp(\text{SIDIS})} = -h_1^\perp. \quad (2.40)$$

We will retain κh_1^\perp in the text for Boer-Mulders function in SIDIS.

For a generic TMD PDF \mathcal{F} and TMD FF \mathcal{D} one has

$$\begin{aligned} \mathcal{D}\mathcal{F} + \bar{\mathcal{D}}\bar{\mathcal{F}} &\equiv \mathcal{D}\left(\frac{1}{\alpha}, \frac{1}{\alpha^2}(\mathbf{q}_T + \mathbf{k}_T)^2\right)\mathcal{F}(-\beta, \mathbf{k}_T^2) + \bar{\mathcal{D}}\left(\frac{1}{\alpha}, \frac{1}{\alpha^2}(\mathbf{q}_T + \mathbf{k}_T)^2\right)\bar{\mathcal{F}}(-\beta, \mathbf{k}_T^2) \\ &= \mathcal{D}(z_h, z_h^2(\mathbf{q}_T + \mathbf{k}_T)^2)\mathcal{F}(x, \mathbf{k}_T^2) + \bar{\mathcal{D}}(z_h, z_h^2(\mathbf{q}_T + \mathbf{k}_T)^2)\bar{\mathcal{F}}(x, \mathbf{k}_T^2). \end{aligned} \quad (2.41)$$

The kinematical tensor structures $\mathcal{W}_{\mu\nu}^{F,H}$ are taken from Ref. [21] and tensors for SIDIS are related to those in DY as follows

$$\begin{aligned} \mathcal{W}_{\mu\nu}^F(q, \mathbf{k}_T) &= {}^{\text{DY}}\mathcal{W}_{\mu\nu}^F(-q, \mathbf{k}_T) = -g_{\mu\nu}^T - \frac{1}{Q^2}(q_\mu^\parallel q_{T\nu} + q_\nu^\parallel q_{T\mu}) + \frac{\mathbf{q}_T^2}{Q^4}q_\mu^\parallel q_\nu^\parallel \\ &+ \frac{\tilde{q}_\mu \tilde{q}_\nu}{Q^4}[\mathbf{q}_T^2 + 4(k, q+k)_T] + \left[\frac{\tilde{q}_\mu}{Q^2} \left(g_{\nu i}^T + \frac{q_\nu^\parallel q_i}{Q^2} \right) (q+2k)_T^i + \mu \leftrightarrow \nu \right] \end{aligned} \quad (2.42)$$

$$\begin{aligned} \mathcal{W}_{\mu\nu}^H(q, \mathbf{k}_T) &= {}^{\text{DY}}\mathcal{W}_{\mu\nu}^H(-q, \mathbf{k}_T) \\ &= \frac{1}{Mm_h} [k_{T\mu}(q+k)_{T\nu} + k_{T\nu}(q+k)_{T\mu} + g_{\mu\nu}^T(k, q+k)_T] + 2\frac{\tilde{q}_\mu \tilde{q}_\nu - q_\mu^\parallel q_\nu^\parallel}{Q^4 M m_h} \mathbf{k}_T^2 (q+k)_T^2 \\ &- \frac{1}{Q^2 M m_h} \left(q_\mu^\parallel [-\mathbf{k}_T^2 (q+k)_{T\nu} + k_{T\nu}(q+k)_T^2] + \tilde{q}_\mu [-\mathbf{k}_T^2 (q+k)_{T\nu} - k_{T\nu}(q+k)_T^2] + \mu \leftrightarrow \nu \right) \\ &+ \frac{\tilde{q}_\mu \tilde{q}_\nu + q_\mu^\parallel q_\nu^\parallel}{Q^4 M m_h} [\mathbf{q}_T^2 + 2(k, q+k)_T] (k, q+k)_T - \frac{q_\mu^\parallel \tilde{q}_\nu + \tilde{q}_\mu q_\nu^\parallel}{Q^4 M m_h} (2k+q, q)_T (k, q+k)_T \end{aligned} \quad (2.43)$$

Here $q_\mu^\parallel \equiv p_1/z_h - x p_2$ and $\tilde{q}_\mu \equiv p_1/z_h + x p_2$.⁴ Notice that the leading-twist contribution is given by the first terms in the R.H.S. of Eq. (2.42) and Eq. (2.43).

It is easy to see that $W_{\mu\nu}^1$ is transverse⁵

$$q^\mu W_{\mu\nu}^1(q) = q^\nu W_{\mu\nu}^1(q) = 0, \quad (2.44)$$

⁴In SIDIS, in our approximation $p_1^\mu = P_h^\mu$ and $p_2^\mu = P^\mu$. Strictly speaking, $Q^2 = -q_\parallel^2 + \mathbf{q}_T^2$ and $-\beta = x + x \frac{\mathbf{q}_T^2}{Q^2}$ but taking into account terms $\sim \mathbf{q}_T^2$ will lead to power corrections $\sim 1/Q^3$.

⁵As discussed in Ref. [21], the second part $W_{\mu\nu}^2$ is also gauge invariant, but $W_{\mu\nu}^3$ is not. To get the “gauge completion” for $W_{\mu\nu}^3$ one needs to take into account $1/Q^3$ corrections.

As we mentioned above, our numerical estimates for the structure functions will be based solely on $W_{\mu\nu}^1$.

3 Structure functions

To obtain structure functions that appear in Eq. (2.6) we use Eqs. (2.85-2.48) from Ref. [17],

$$F_{UU,T} = \frac{x}{4z_h} (\mathcal{S}_1^{\mu\nu} - \mathcal{S}_0^{\mu\nu}) W_{\mu\nu} = \frac{1}{2} F_{UU,L} - \frac{x}{4z_h} \mathcal{S}_0^{\mu\nu} W_{\mu\nu}, \quad (3.1)$$

$$F_{UU,L} = \frac{x}{4z_h} 2\mathcal{S}_1^{\mu\nu} W_{\mu\nu}, \quad (3.2)$$

$$F_{UU}^{\cos \phi_h} = \frac{x}{4z_h} \mathcal{S}_3^{\mu\nu} W_{\mu\nu}, \quad (3.3)$$

$$F_{UU}^{\cos 2\phi_h} = \frac{x}{4z_h} (\mathcal{S}_0^{\mu\nu} - \mathcal{S}_1^{\mu\nu} - 2\mathcal{S}_2^{\mu\nu}) W_{\mu\nu} = -\frac{1}{2} F_{UU,L} + \frac{x}{4z_h} (\mathcal{S}_0^{\mu\nu} - 2\mathcal{S}_2^{\mu\nu}) W_{\mu\nu}. \quad (3.4)$$

Here, in our notations, we have

$$\mathcal{S}_0^{\mu\nu} = g^{\mu\nu} - \frac{q^\mu q^\nu}{q^2}, \quad (3.5)$$

$$\mathcal{S}_1^{\mu\nu} = \frac{(\tilde{q}^\mu + \check{q}^\nu)(\tilde{q}^\nu + \check{q}^\mu)}{-q^2}, \quad (3.6)$$

$$\mathcal{S}_2^{\mu\nu} = \frac{\check{q}^\mu \check{q}^\nu}{-\mathbf{q}_T^2}, \quad (3.7)$$

$$\mathcal{S}_3^{\mu\nu} = \frac{(\tilde{q}^\mu + \check{q}^\mu)\check{q}^\nu + \mu \leftrightarrow \nu}{q_T Q}, \quad (3.8)$$

where the vectors are defined as

$$\tilde{q}^\mu = \alpha p_1^\mu - \beta p_2^\mu = \frac{P_h^\mu}{z_h} + x \left(1 - \frac{\mathbf{q}_T^2}{Q^2} \right) P^\mu, \quad (3.9)$$

$$\check{q}^\mu = q_T^\mu + \frac{2\mathbf{q}_T^2}{Q^2} p_2^\mu = q_T^\mu + \frac{2\mathbf{q}_T^2}{Q^2} P^\mu. \quad (3.10)$$

Using our ‘‘gauge completion of the leading twist’’ approximation, we obtain

$$F_{UU,T} = x \sum_a H_{aa}(Q^2, \mu^2) \int d^2 \mathbf{k}_T \left[\left(1 - \frac{2\mathbf{q}_T \cdot \mathbf{k}_T}{Q^2} \right) f_1(x, \mathbf{k}_T^2) D_1(z_h, ((\mathbf{q}_T + \mathbf{k}_T)z_h)^2) + \right. \\ \left. - \frac{2\mathbf{k}_T^2}{Mm_h Q^2} \mathbf{q}_T \cdot (\mathbf{q}_T + \mathbf{k}_T) h_1^\perp(x, \mathbf{k}_T^2) H_1^\perp(z_h, ((\mathbf{q}_T + \mathbf{k}_T)z_h)^2) \right], \quad (3.11)$$

$$F_{UU,L} = x \sum_a H_{aa}(Q^2, \mu^2) \int d^2 \mathbf{k}_T \left[\frac{4\mathbf{k}_T^2}{Q^2} f_1(x, \mathbf{k}_T^2) D_1(z_h, ((\mathbf{q}_T + \mathbf{k}_T)z_h)^2) \right. \\ \left. + \frac{4\mathbf{k}_T^2}{Mm_h Q^2} \mathbf{k}_T \cdot (\mathbf{q}_T + \mathbf{k}_T) h_1^\perp(x, \mathbf{k}_T^2) H_1^\perp(z_h, ((\mathbf{q}_T + \mathbf{k}_T)z_h)^2) \right], \quad (3.12)$$

$$F_{UU}^{\cos \phi_h} = x \sum_a H_{aa}(Q^2, \mu^2) \int d^2 \mathbf{k}_T \left[\frac{2\mathbf{q}_T \cdot \mathbf{k}_T}{Qq_T} f_1(x, \mathbf{k}_T^2) D_1(z_h, ((\mathbf{q}_T + \mathbf{k}_T)z_h)^2) \right. \\ \left. + \frac{2\mathbf{k}_T^2}{Mm_h Qq_T} \mathbf{q}_T \cdot (\mathbf{q}_T + \mathbf{k}_T) h_1^\perp(x, \mathbf{k}_T^2) H_1^\perp(z_h, ((\mathbf{q}_T + \mathbf{k}_T)z_h)^2) \right], \quad (3.13)$$

$$F_{UU}^{\cos 2\phi_h} = x \sum_a H_{aa}(Q^2, \mu^2) \int d^2 \mathbf{k}_T \left[-\frac{2\mathbf{q}_T \cdot \mathbf{k}_T}{Q^2} f_1(x, \mathbf{k}_T^2) D_1(z_h, ((\mathbf{q}_T + \mathbf{k}_T)z_h)^2) \right. \\ \left. + \left(-\frac{\mathbf{k}_T \cdot (\mathbf{q}_T + \mathbf{k}_T)}{Mm_h} + \frac{2\mathbf{k}_T \cdot \mathbf{q}_T (\mathbf{q}_T \cdot (\mathbf{q}_T + \mathbf{k}_T))}{\mathbf{q}_T^2 Mm_h} \right) \right]$$

$$-\frac{2\mathbf{k}_T^2(\mathbf{q}_T \cdot (\mathbf{q}_T + \mathbf{k}_T))}{Q^2 M m_h} \Big) h_1^\perp(x, \mathbf{k}_T^2) H_1^\perp(z_h, ((\mathbf{q}_T + \mathbf{k}_T) z_h)^2) \Big], \quad (3.14)$$

Notice that in the formulas above, Boer-Mulders functions are for Drell-Yan.

We now rewrite Eqs. (3.11-3.14) in the standard notations of Eqs. (2.12) using Eq. (2.11), $-\mathbf{p}_\perp/z_h = \mathbf{q}_T + \mathbf{k}_T$ and $\hat{\mathbf{h}} = -\mathbf{q}_T/q_T$, and using Boer-Mulders functions for SIDIS, κh_1^\perp with $\kappa = -1$,

$$F_{UU,T} = \mathcal{C} \left[\left(1 + \frac{2q_T}{Q^2} (\hat{\mathbf{h}} \cdot \mathbf{k}_\perp) \right) f_1(x, \mathbf{k}_\perp^2) D_1(z_h, \mathbf{p}_\perp^2) + \frac{2q_T \mathbf{k}_\perp^2}{z_h M m_h Q^2} (\hat{\mathbf{h}} \cdot \mathbf{p}_\perp) \kappa h_1^\perp(x, \mathbf{k}_\perp^2) H_1^\perp(z_h, \mathbf{p}_\perp^2) \right], \quad (3.15)$$

$$F_{UU,L} = \mathcal{C} \left[\frac{4\mathbf{k}_\perp^2}{Q^2} f_1 D_1 + \frac{4\mathbf{k}_\perp^2}{z_h M m_h Q^2} (\mathbf{k}_\perp \cdot \mathbf{p}_\perp) \kappa h_1^\perp H_1^\perp \right], \quad (3.16)$$

$$F_{UU}^{\cos \phi_h} = \mathcal{C} \left[-\frac{2(\hat{\mathbf{h}} \cdot \mathbf{k}_\perp)}{Q} f_1 D_1 - \frac{2\mathbf{k}_\perp^2}{z_h M m_h Q} (\hat{\mathbf{h}} \cdot \mathbf{p}_\perp) \kappa h_1^\perp H_1^\perp \right], \quad (3.17)$$

$$F_{UU}^{\cos 2\phi_h} = \mathcal{C} \left[\frac{2q_T(\hat{\mathbf{h}} \cdot \mathbf{k}_\perp)}{Q^2} f_1 D_1 - \left(\frac{(\mathbf{k}_\perp \cdot \mathbf{p}_\perp)}{z_h M m_h} - \frac{2(\hat{\mathbf{h}} \cdot \mathbf{k}_\perp)(\hat{\mathbf{h}} \cdot \mathbf{p}_\perp)}{z_h M m_h} \right) \kappa h_1^\perp H_1^\perp + \frac{2q_T \mathbf{k}_\perp^2}{z_h M m_h Q^2} (\hat{\mathbf{h}} \cdot \mathbf{p}_\perp) \kappa h_1^\perp H_1^\perp \right], \quad (3.18)$$

For the NNLP contributions, $\sim 1/Q^2$, in these equations one obtains the following relations:

$$F_{UU,T}^{\text{NNLP}} = F_{UU}^{\cos 2\phi_h \text{NNLP}} = -\frac{q_T}{Q} F_{UU}^{\cos \phi_h}. \quad (3.19)$$

TMDs are often studied in b_T space and the convolutions can be written in terms of Fourier transformations. We express the convolutions in Eq. (3.15), (3.16), (3.17), and (3.18) through Fourier transforms of products of TMDs in b_T space [31], where the Fourier transform is defined as, see Ref. [9],

$$\mathcal{B}[\tilde{f}^{(m)} \tilde{D}^{(n)}] \equiv x \sum_a H_{aa}(Q^2, \mu^2) \int_0^\infty \frac{db_T}{2\pi} b_T b_T^{m+n} J_{m+n}(q_T b_T) \times \tilde{f}^{(m)}(x, b_T) \tilde{D}^{(n)}(z_h, b_T). \quad (3.20)$$

The Fourier-transformed TMD PDFs \tilde{f} and MD FFs \tilde{D} and their derivatives $\tilde{f}^{(n)}$ and $\tilde{D}^{(n)}$ are defined as, see e.g. Ref. [9, 31],

$$\begin{aligned} \tilde{f}^{(n)}(x, b_T) &\equiv n! \left(\frac{-1}{M^2 b_T} \partial_{b_T} \right)^n \tilde{f}(x, b_T) \\ &= \frac{2\pi n!}{(M^2)^n} \int_0^\infty dk_\perp k_\perp \left(\frac{k_\perp}{b_T} \right)^n J_n(b_T k_\perp) f(x, k_\perp), \end{aligned} \quad (3.21)$$

$$\begin{aligned} \tilde{D}^{(n)}(z_h, b_T) &\equiv n! \left(\frac{-1}{m_h^2 b_T} \partial_{b_T} \right)^n \tilde{D}(z, b_T) \\ &= \frac{2\pi n!}{(m_h^2)^n} \int_0^\infty \frac{dp_\perp p_\perp}{z_h^2} \left(\frac{p_\perp}{z_h b_T} \right)^n J_n \left(\frac{b_T p_\perp}{z_h} \right) D(z_h, p_\perp). \end{aligned} \quad (3.22)$$

We obtain:

$$F_{UU,T} = \mathcal{B}[\tilde{f}_1^{(0)} \tilde{D}_1^{(0)}] + \frac{2q_T M^2}{Q^2} \mathcal{B}[\tilde{f}_1^{(1)} \tilde{D}_1^{(0)}] + \frac{2q_T m_h}{Q^2 M} \mathcal{B} \left[\widetilde{k_\perp^2 \kappa h_1^\perp}^{(0)} \tilde{H}_1^{(1)} \right], \quad (3.23)$$

$$F_{UU,L} = \frac{4}{Q^2} \mathcal{B} \left[\widetilde{k_\perp^2 f_1^{(0)}} \tilde{D}_1^{(0)} \right] - \frac{4m_h M}{Q^2} \mathcal{B}' \left[\widetilde{k_\perp^2 \kappa h_1^\perp}^{(1)} \tilde{H}_1^{\perp(1)} \right], \quad (3.24)$$

$$F_{UU}^{\cos \phi_h} = -\frac{2M^2}{Q} \mathcal{B} \left[\widetilde{f_1^{(1)}} \tilde{D}_1^{(0)} \right] - \frac{2m_h}{QM} \mathcal{B} \left[\widetilde{k_\perp^2 \kappa h_1^\perp}^{(0)} \tilde{H}_1^{\perp(1)} \right], \quad (3.25)$$

$$F_{UU}^{\cos 2\phi_h} = Mm_h \mathcal{B} \left[\widetilde{\kappa h_1^\perp}^{(1)} \tilde{H}_1^{\perp(1)} \right] + \frac{2q_T M^2}{Q^2} \mathcal{B} \left[\widetilde{f_1^{(1)}} \tilde{D}_1^{(0)} \right] + \frac{2q_T m_h}{Q^2 M} \mathcal{B} \left[\widetilde{k_\perp^2 \kappa h_1^\perp}^{(0)} \tilde{H}_1^{\perp(1)} \right], \quad (3.26)$$

where we define a new convolution:

$$\begin{aligned} \mathcal{B}'[\tilde{f}^{(m)} \tilde{D}^{(n)}] &\equiv x \sum_a H_{aa}(Q^2, \mu^2) \int_0^\infty \frac{db_T}{2\pi} b_T b_T^{m+n} J_0(q_T b_T) \\ &\quad \times \tilde{f}^{(m)}(x, b_T) \tilde{D}^{(n)}(z_h, b_T). \end{aligned} \quad (3.27)$$

The functions $\widetilde{k_\perp^2 f}^{(0)}$ and $\widetilde{k_\perp^2 f}^{(1)}$ are defined as

$$\widetilde{k_\perp^2 f}^{(n)}(x, b_T) \equiv \frac{2\pi n!}{(M^2)^n} \int_0^\infty dk_\perp k_\perp \left(\frac{k_\perp}{b_T} \right)^n J_n(b_T k_\perp) \mathbf{k}_\perp^2 f(x, \mathbf{k}_\perp^2). \quad (3.28)$$

These formulas can facilitate numerical studies if TMDs are expressed in b_T rather than k_\perp space.

4 Numerical estimates and comparisons

In this Section we will provide numerical estimates for structure functions and will compare our results to the existing literature, in particular to two recent papers: Piloñeta and Vladimirov Ref. [17]; Ebert, Gao, and Stewart Ref. [13], and previous literature, Bacchetta et al Ref. [2], generalized helicity formalism by Anselmino et al [32], and other papers. Piloñeta and Vladimirov Ref. [17] studied the kinematic power corrections to SIDIS for all unpolarized and polarized structure functions, those corrections scale as k_\perp/Q . Ebert, Gao, and Stewart Ref. [13] studied NLP contributions to SIDIS, kinematic corrections and subleading contribution due to hard scattering and subleading SCET_{II} Lagrangian insertions. They present the NLP corrections for the unpolarized and polarized structure functions that start from NLP, for the unpolarized case it is $F_{UU}^{\cos \phi_h}$. Anselmino et al [32] considers a simple parton model and keeps exact kinematics of on-shell quarks at the level of quark scattering. Even though expansion is possible, the formulas in Ref. [32] contain usually LP terms only. For the convenience of the reader we list conversions of notations used in those papers to our notations in Appendix A.

Our approximation consists in keeping the terms from $L^{\mu\nu}W_{\mu\nu}^1$ that proved to be useful for Drell-Yan, see Ref. [29]. Further improvements can be made by inclusion of the terms from $L^{\mu\nu}W_{\mu\nu}^2$ and $L^{\mu\nu}W_{\mu\nu}^3$. We will not perform a complete phenomenological analysis or extraction of TMDs, but rather present useful estimates that demonstrate the impact of the next-to-leading power corrections in Semi-Inclusive Deep Inelastic Scattering process. For simplicity of the numerical estimates, we will utilize the generalized parton model for TMDs. It was proven to give a reasonable description of multiplicities and asymmetries observed in SIDIS [33–42], but lacks certain sophistication of the theory, such as the complete treatment of the TMD evolution. As we are going to estimate power corrections, the logarithmic dependence due to the evolution is not going to be very important at this stage.

We will use the following parametrizations for TMDs

$$f_1^a(x, \mathbf{k}_\perp^2) = f_1^a(x) \frac{1}{\pi \langle k_\perp^2 \rangle_{f_1}} e^{-\mathbf{k}_\perp^2 / \langle k_\perp^2 \rangle_{f_1}}, \quad (4.1a)$$

$$D_1^a(z_h, \mathbf{p}_\perp^2) = D_1^a(z_h) \frac{1}{\pi \langle p_\perp^2 \rangle_{D_1}} e^{-\mathbf{p}_\perp^2 / \langle p_\perp^2 \rangle_{D_1}}, \quad (4.1b)$$

$$H_1^{\perp a}(z_h, \mathbf{p}_\perp^2) = H_1^{\perp(1)a}(z_h) \frac{2z^2 m_h^2}{\pi \langle p_\perp^2 \rangle_{H_1^\perp}^2} e^{-\mathbf{p}_\perp^2 / \langle p_\perp^2 \rangle_{H_1^\perp}}, \quad (4.1c)$$

$$h_1^{\perp a}(x, \mathbf{k}_\perp^2) = h_1^{\perp(1)a}(x) \frac{2M^2}{\pi \langle k_\perp^2 \rangle_{h_1^\perp}^2} e^{-\mathbf{k}_\perp^2 / \langle k_\perp^2 \rangle_{h_1^\perp}}. \quad (4.1d)$$

These parametrizations were shown to work reasonably well in phenomenological applications. The collinear functions $f_1^a(x)$ and $D_1^a(z)$ are taken from MSTW [43] and DSS [44] extractions [33–42]. This is the same set up as in Ref. [25] where Semi-Inclusive Deep Inelastic Scattering in Wandzura-Wilczek-type (WW) approximation was studied. In this approximation, TMD functions that originate from quark-gluon correlations are assumed to be small and a series of relations are found among TMDs. These relations, such as $xf_1^\perp \simeq f_1$ and $xh \simeq -(\mathbf{k}_\perp^2/M^2)h_1^\perp$, see Appendix B, allow to reduce drastically the number of TMDs contributing to structure functions and to simplify the expressions. It was found in Ref. [25] that WW approximations were generally in agreement with the experimental observations. By keeping the same set up we will be able to comment on similarities and differences of WW approximations with our formalism.

Parametrizations for unpolarized TMD PDF and TMD FF will be taken from Ref. [33], they are flavor independent with $\langle k_\perp^2 \rangle_{f_1} = 0.25$ (GeV 2), $\langle p_\perp^2 \rangle_{D_1} = 0.2$ (GeV 2). As we do not perform a phenomenological analysis, these parametrizations are sufficient for numerical estimates. Using formulas (3.15)–(3.18) one can perform calculations with any other set of TMD PDFs and TMD FFs. Boer-Mulders functions and their first moments, $h_1^{\perp(1)}(x)$, are taken from Ref. [45] and the Collins FF and their first moments, $H_1^{\perp(1)}(z_h)$, are from Ref. [46]. This set up will allow us to have the direct comparison with results of Ref. [25]. In the plots in the following Sections we will not restrict the range of $P_{h\perp}$ to the one where our approximation works, $q_T/Q \ll 1$. The reason is that, first, experimental values of q_T are not always available and, second, we would like to explore the expression for the whole range in $P_{h\perp}$, however the interpretation of our estimates at large values of $P_{h\perp}$ should be done with caution.

Notice that it was fund in Ref. [45] that both u and d first moments of Boer-Mulders functions are negative in SIDIS. Collins FF for u quark fragmentation into π^+ is positive, while d quark fragmentation into π^+ is negative, see e.g. Ref. [46].

4.1 $F_{UU,T}$ structure function

Our result for $F_{UU,T}$, Eq. (3.15), shows that it has LP and NNLP contributions, while NLP contribution is absent,

$$F_{UU,T} = F_{UU,T}^{\text{LP}} + F_{UU,T}^{\text{NNLP}}, \quad (4.2)$$

$$F_{UU,T} = \mathcal{C}[f_1 D_1] + \mathcal{C}\left[\frac{2q_T}{Q^2}(\hat{\mathbf{h}} \cdot \mathbf{k}_\perp) f_1 D_1\right] + \mathcal{C}\left[\frac{2q_T \mathbf{k}_\perp^2}{z_h M m_h Q^2}(\hat{\mathbf{h}} \cdot \mathbf{p}_\perp) \kappa h_1^\perp H_1^\perp\right], \quad (4.3)$$

where the first term in Eq. (4.3) contains the standard leading power result,

$$F_{UU,T}^{\text{LP}} = \mathcal{C}[f_1 D_1], \quad (4.4)$$

see Refs [2, 9]. The next-to-next-to-leading power contributions $F_{UU,T}^{\text{NNLP}}$, the second and the third terms in Eq. (4.3) proportional to $1/Q^2$, are the main results of our study. This formula appears to have a slightly different structure comparing to Ref. [17], see Eq. (B.3) from Ref. [17]:

$$F_{UU,T}|_{\text{Ref.}[17]} = \mathcal{C}[f_1 D_1] + \frac{1}{2} F_{UU,L}, \quad (4.5)$$

where $F_{UU,L}$ is discussed in the next Section. The difference of our result and Ref. [17] is due to different results for $\mathcal{S}_0^{\mu\nu} W_{\mu\nu}$ in two formalisms.

In order to provide numerical estimates we will use parametrizations from Eqs. (4.1a) and (4.1b). We obtain the following expressions

$$F_{UU,T}^{\text{LP}}(x, z_h, P_{h\perp}) = x \sum_a e_a^2 f_1^a(x) D_1^a(z_h) \frac{\exp(-P_{h\perp}^2/(z_h^2 \langle k_\perp^2 \rangle_{f_1} + \langle p_\perp^2 \rangle_{D_1}))}{\pi (z_h^2 \langle k_\perp^2 \rangle_{f_1} + \langle p_\perp^2 \rangle_{D_1})}, \quad (4.6)$$

and

$$\begin{aligned} F_{UU,T}^{\text{NNLP}}(x, z_h, P_{h\perp}) = & x \sum_a e_a^2 f_1^a(x) D_1^a(z_h) \frac{2 \langle k_\perp^2 \rangle_{f_1} P_{h\perp}^2}{Q^2} \frac{\exp(-P_{h\perp}^2/(z_h^2 \langle k_\perp^2 \rangle_{f_1} + \langle p_\perp^2 \rangle_{D_1}))}{\pi (z_h^2 \langle k_\perp^2 \rangle_{f_1} + \langle p_\perp^2 \rangle_{D_1})^2} \\ & + x \sum_a e_a^2 h_1^{\perp(1)a}(x) H_1^{\perp(1)a}(z_h) \frac{\lambda P_{h\perp}^2}{Q^2} \frac{\exp(-P_{h\perp}^2/(z_h^2 \langle k_\perp^2 \rangle_{H_1^\perp} + \langle p_\perp^2 \rangle_{H_1^\perp}))}{\pi (z_h^2 \langle k_\perp^2 \rangle_{H_1^\perp} + \langle p_\perp^2 \rangle_{H_1^\perp})^4}, \end{aligned} \quad (4.7)$$

where $\lambda = 8Mm_h(\langle p_\perp^2 \rangle_{H_1^\perp}^2 + z_h^2 \langle k_\perp^2 \rangle_{H_1^\perp} (P_{h\perp}^2 - z_h^2 \langle k_\perp^2 \rangle_{H_1^\perp}))$.

In Fig. 3 we show various contributions to $F_{UU,T}$ for the pion production off the proton at characteristic kinematical variables $Q^2 = 3 \text{ GeV}^2$, $x = 0.2$, $z_h = 0.3$. One can see that $F_{UU,T}^{\text{NNLP}}$ is dominated by the contribution from $f_1 D_1$, second term in Eq. (4.3). Contributions from $h_1^\perp H_1^\perp$, third term in Eq. (4.3), have opposite signs and approximately same magnitudes for π^+ and π^- , see the left panel of Fig. 3. We will show the comparison to experimental data in the following Section.

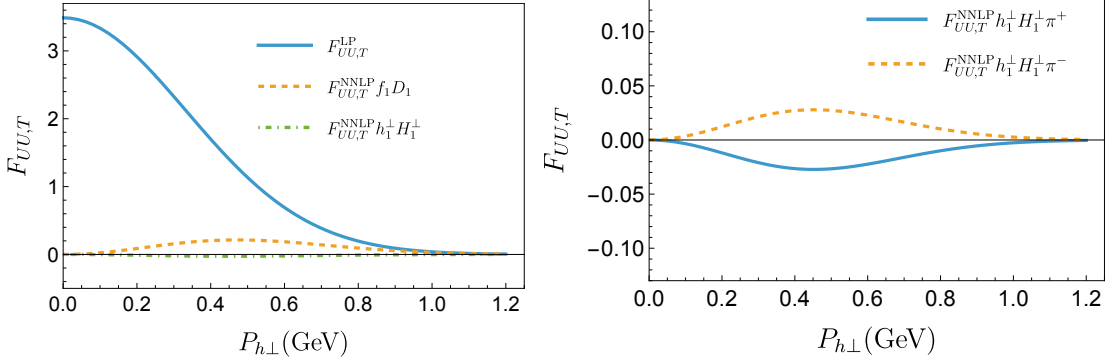


Figure 3: $F_{UU,T}$ structure function for pion production off the proton at $Q^2 = 3 \text{ GeV}^2$, $x = 0.2$, $z_h = 0.3$. Left panel shows π^+ leading power contribution (blue line), next-to-next-to-leading power contribution from $f_1 D_1$ (orange dashed line), and from $h_1^\perp H_1^\perp$ (green dot-dashed line). Right panel shows next-to-next-to-leading power contribution from $h_1^\perp H_1^\perp$ for π^+ (blue line) and π^- (orange dashed line) production.

The ratio $F_{UU,T}$ structure function over the leading power $F_{UU,T}^{\text{LP}}$ for π^+ production off the proton at three values for Q^2 and $x = 0.2$, $z_h = 0.3$ is shown in Fig. 4. One can see that the next-to-next-to-leading power contribution becomes large at large values of $P_{h\perp}$, even surpassing the leading power contribution at large $P_{h\perp}$ for relatively low values of Q^2 . Even for the largest $Q^2 = 20 \text{ GeV}^2$ shown in Fig. 4, the ratio can be around 10%. As experiments often operate with low to moderate values of Q^2 we conclude that it is important to take into account next-to-next-to-leading power contributions for $F_{UU,T}$ in phenomenological analyses of the experimental data. In addition, taking into account $F_{UU,T}^{\text{NNLP}}$ will be important for transition region from TMD to collinear description of the experimental data that will happen in the region of $q_T \sim Q$.

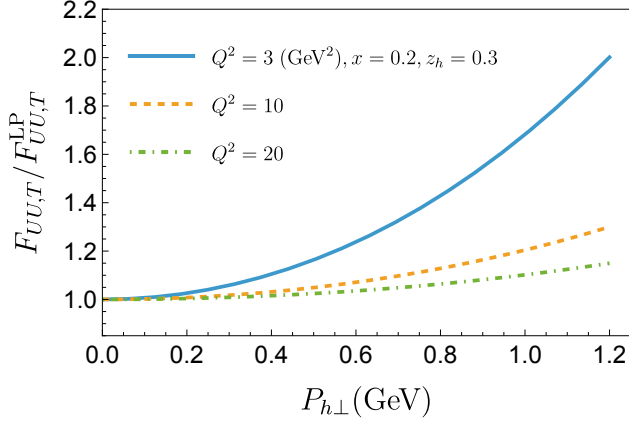


Figure 4: The ratio of $F_{UU,T}$ structure function over the leading power $F_{UU,T}^{\text{LP}}$ for π^+ production off the proton at $Q^2 = 3 \text{ GeV}^2$, $x = 0.2$, $z_h = 0.3$.

4.2 $F_{UU,L}$ structure function

Our result for $F_{UU,L}$ structure function, that starts from next-to-next-to-leading power, Eq. (3.16), reads

$$F_{UU,L} = \mathcal{C} \left[\frac{4\mathbf{k}_\perp^2}{Q^2} f_1 D_1 \right] + \mathcal{C} \left[\frac{4\mathbf{k}_\perp^2}{z_h M m_h Q^2} (\mathbf{k}_\perp \cdot \mathbf{p}_\perp) \kappa h_1^\perp H_1^\perp \right]. \quad (4.8)$$

It is the same as the result in Pilóneta and Vladimirov, Ref. [17], see Eq. (B.4) from Ref. [17], calculated for large Q^2 . $F_{UU,L}$ appears only at next-to-next-to-leading power and therefore was not used previously in phenomenology of TMDs. Nevertheless, the first term in Eq. (4.8) was known and calculated in Bacchetta et al Ref. [3], see Eq.(6.15) of Ref. [3], using a generalized parton model of Anselmino et al in Ref. [33]. In Ref. [33] the intrinsic transverse momentum is included in distribution and fragmentation functions and the kinematics is taken such that the quarks in the parton sub-process of quark scattering are on the mass shell. It is remarkable, but not surprising, that the parton model considered in Ref. [33] gives correct results for the kinematical next-to-next-to-leading power contribution to $F_{UU,L}$ and, as we will see in the following sections, for $F_{UU}^{\cos 2\phi_h}$ and $F_{UU}^{\cos \phi_h}$. Notice that Ref. [33] was later developed as generalized helicity formalism by Anselmino et al in Ref. [32] and was shown to coincide in kinematical contributions with standard results, such as Ref. [2].

There exists a considerable experimental interest to study $F_{UU,L}$. The ratio

$$R_{\text{SIDIS}} = \frac{F_{UU,L}}{F_{UU,T}} \quad (4.9)$$

is planned to be studied at Jefferson Lab by experiments E12-06-104, E12-09-017, E12-09-002 in Hall C and Hall B, and the first data from HALL C have already appeared in Ref. [11].

We obtain the following parametrization for $F_{UU,L}$:

$$F_{UU,L}(x, z_h, P_{h\perp}) = x \sum_a e_a^2 f_1^a(x) D_1^a(z_h) \frac{\lambda_1}{Q^2} \frac{\exp(-P_{h\perp}^2/(z_h^2 \langle k_\perp^2 \rangle_{f_1} + \langle p_\perp^2 \rangle_{D_1}))}{\pi (z_h^2 \langle k_\perp^2 \rangle_{f_1} + \langle p_\perp^2 \rangle_{D_1})^3} \\ - x \sum_a e_a^2 h_1^{\perp(1)a}(x) H_1^{\perp(1)a}(z_h) \frac{\lambda_2}{Q^2} \frac{\exp(-P_{h\perp}^2/(z_h^2 \langle k_\perp^2 \rangle_{h_1^\perp} + \langle p_\perp^2 \rangle_{H_1^\perp}))}{\pi (z_h^2 \langle k_\perp^2 \rangle_{h_1^\perp} + \langle p_\perp^2 \rangle_{H_1^\perp})^5}, \quad (4.10)$$

where $\lambda_1 = 4 \langle k_\perp^2 \rangle_{f_1} (\langle p_\perp^2 \rangle_{D_1}^2 + z_h^2 \langle k_\perp^2 \rangle_{f_1} (P_{h\perp}^2 + \langle p_\perp^2 \rangle_{D_1}))$ and $\lambda_2 = 16 M m_h z_h^2 (-\langle k_\perp^2 \rangle_{h_1^\perp} P_{h\perp}^4 z_h^2 + 2 \langle p_\perp^2 \rangle_{H_1^\perp} (\langle p_\perp^2 \rangle_{H_1^\perp} + z_h^2 \langle k_\perp^2 \rangle_{h_1^\perp})^2 - 2 P_{h\perp}^2 (\langle p_\perp^2 \rangle_{H_1^\perp}^2 - z_h^4 \langle k_\perp^2 \rangle_{h_1^\perp}^2))$.

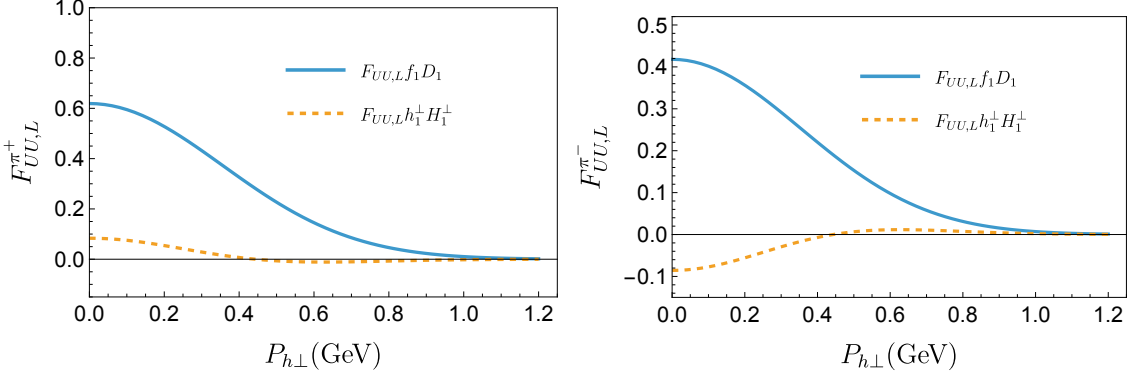


Figure 5: $F_{UU,L}$ for π^+ (left panel) and π^- (right panel) production off the proton at $Q^2 = 5$ GeV^2 and $x = 0.2$, $z_h = 0.3$. The contribution from the first term in Eq. (4.8), convolution of $f_1 D_1$, is shown as blue line, the second term convolution of $h_1^\perp D_1^\perp$ in Eq. (4.8) is shown as orange dashed line.

Our numerical estimates of $F_{UU,L}$ for π^+ and π^- production off the proton at $Q^2 = 5$ GeV^2 at $x = 0.2$, $z_h = 0.3$ are shown in Fig. 5. One can see that the contribution from the first term in Eq. (4.8) is always positive, it is around 20% of $F_{UU,T}$ at this Q^2 . The second term, proportional to $h_1^\perp D_1^\perp$, changes sign between π^+ and π^- and is comparable in magnitude to the first term. It means that there may be differences in experimental results for π^+ and π^- production. Notice that the term proportional to $h_1^\perp D_1^\perp$ gives zero if integrated over $P_{h\perp}$, therefore we expect to observe these differences in $P_{h\perp}$ dependent measurements only.

We show our estimates for R_{SIDIS} in Fig. 6 where we observe that the values for the ratio are different for π^+ and π^- production due to the term containing $h_1^\perp H_1^\perp$ that has opposite sign for π^+ and π^- . We predict this ratio to be around 20% in the kinematical range of Jefferson Lab. R_{SIDIS} can also be studied at the Electron-Ion Collider at higher values of Q . The Electron-Ion Collider data will allow to study the transition region from low to high q_T . Our estimates are in general agreement with those presented in Ref. [47], however we expect a strong dependence on the charge of the pion.

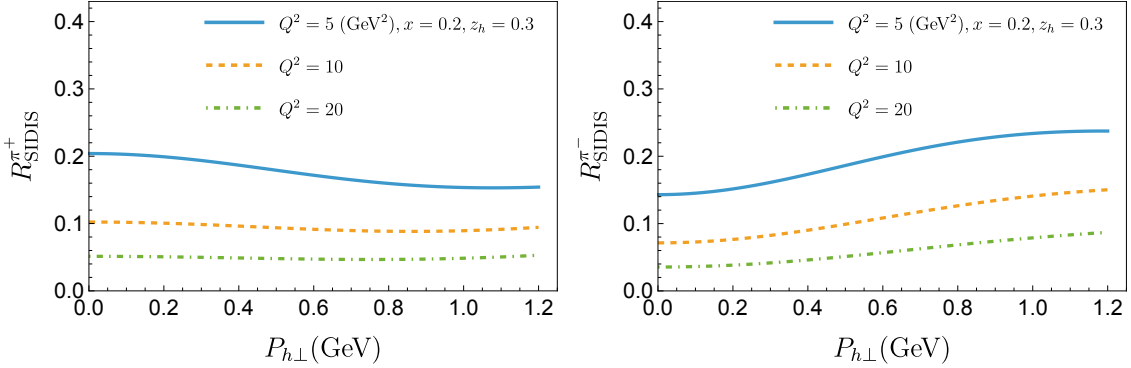


Figure 6: R_{SIDIS} for π^+ (left panel) and π^- (right panel) production off the proton at $Q^2 = 5, 10, 20$ GeV^2 and $x = 0.2$, $z_h = 0.3$.

At this point it is interesting to compare our results to the existing experimental data. HERMES experiment measured multiplicities for pion and kaon production in the scattering of 27.6 GeV

electrons or positrons of HERA's polarized lepton storage ring off proton and deuteron targets. The HERMES multiplicity is defined as [48]

$$M_n^h(x, z_h, P_{h\perp}) \equiv \frac{d\sigma_{\text{SIDIS}}(x, z_h, P_{h\perp})/dx dz_h dP_{h\perp}}{d\sigma_{\text{DIS}}(x)/dx} = 2\pi P_{h\perp} \frac{F_{UU,T} + p_1 F_{UU,L}}{x \sum_q e_q^2 f_1^q(x)}. \quad (4.11)$$

In this formula, the second term $p_1 F_{UU,L}$ was not taken into account in the TMD related studies. We present our numerical estimates to two characteristic bins with moderate and high Q^2 in Fig. 7 on the proton target [48], the left panel shows the estimate for π^+ production at $\langle Q^2 \rangle = 2.87 \text{ (GeV}^2)$, $\langle x \rangle = 0.15$, $\langle z \rangle = 0.22$, while the right panel shows the estimate for π^- production at $\langle Q^2 \rangle = 9.2 \text{ (GeV}^2)$, $\langle x \rangle = 0.41$, $\langle z \rangle = 0.22$. The estimates including $F_{UU,T}$ and $F_{UU,L}$ at to next-to-next-to-leading power are shown in blue, while the calculations including only $F_{UU,T}$ at leading power are shown as orange dashed lines. One can see that at moderate values of Q^2 the NNLP contributions are substantial and would influence the phenomenological results. It demonstrates the importance of accounting for NNLP contributions in the future studies. These contributions may be important in resolution of the normalization puzzle found in SIDIS in Ref. [49]. Notice that the collinear cross section $d\sigma_{\text{DIS}}/dx$ also contains contributions due to the longitudinally polarized photons that will be needed to be taken into account in phenomenological studies, we neglect this contribution here for simplicity.

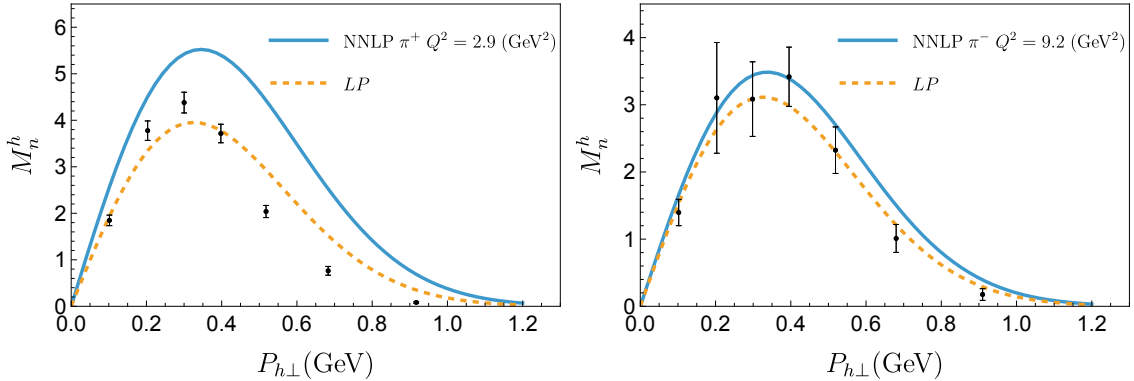


Figure 7: SIDIS multiplicity measured by HERMES [48] for π^+ (right panel) and π^- (left panel) production off the proton target. Calculations shown as blue lines include NNLP contributions, the orange dashed lines include only leading power terms.

Finally, we show representative plots from the COMPASS experiment where charged pions, kaons, or hadrons were measured with 160 GeV longitudinally polarized muons scattered off proton and deuteron targets. The multiplicity measured by COMPASS reads

$$n^h(x, z_h, P_{h\perp}^2) \equiv \frac{d\sigma_{\text{SIDIS}}(x, z, P_{h\perp}^2)/dx dz dP_{h\perp}^2}{d\sigma_{\text{DIS}}(x)/dx} = \pi \frac{F_{UU,T} + p_1 F_{UU,L}}{x \sum_q e_q^2 f_1^q(x)}. \quad (4.12)$$

Left panel of Fig. 8 shows the COMPASS multiplicity [50] at $\langle Q^2 \rangle = 20 \text{ GeV}^2$, $\langle x \rangle = 0.15$, $\langle z \rangle = 0.2$ for h^+ production on the deuteron target. Right panel of Fig. 8 shows the COMPASS multiplicity [50] at $\langle Q^2 \rangle = 2.5 \text{ GeV}^2$, $\langle x \rangle = 0.05$, $\langle z \rangle = 0.4$ for h^- production on the deuteron target. One can see that even at COMPASS energy NNLP contributions are substantial, especially for low values of Q^2 . In order to calculate the multiplicity we assumed that charged hadrons are dominated by pions and we used the same parameters for TMD PDF and TMD FF and we used for previous calculations, one can see that our simple model does not capture well the structure of the COMPASS data.

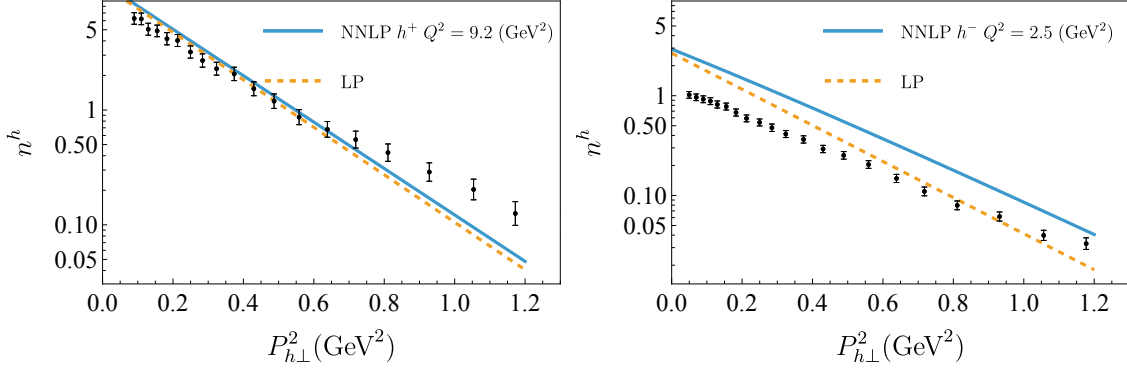


Figure 8: SIDIS multiplicity measured by COMPASS [50] for h^+ (right panel) and h^- (left panel) production off the deuterium target. Calculations shown as blue lines include NNLP contributions, the orange dashed lines include only leading power terms.

We conclude at this point that taking into account the longitudinal structure function $F_{UU,L}$ is important in phenomenological applications. In order to further demonstrate it in Fig. 9 we plot the ratio $F_{UU,T} + p_1 F_{UU,L}$ structure functions over the leading power $F_{UU,T}^{\text{LP}}$ for π^+ production off the proton at $Q^2 = 3 \text{ GeV}^2$, $x = 0.2$, $z_h = 0.3$. One can see, compare to Fig. 4, that the $F_{UU,L}$ is not negligible even at small values of $P_{h\perp}$.

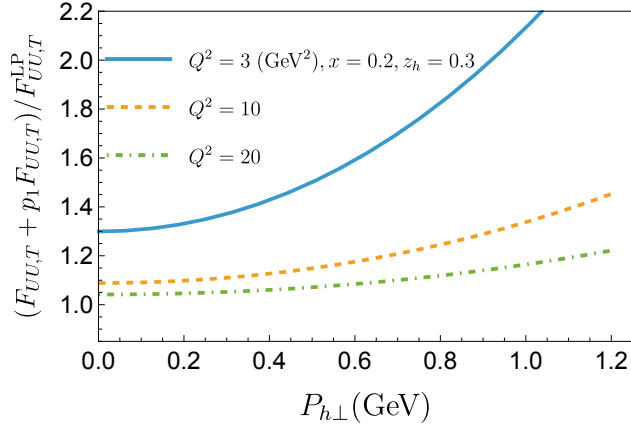


Figure 9: The ratio of $F_{UU,T} + p_1 F_{UU,L}$ structure functions over the leading power $F_{UU,T}^{\text{LP}}$ for π^+ production off the proton at $Q^2 = 3 \text{ GeV}^2$, $x = 0.2$, $z_h = 0.3$.

4.3 $F_{UU}^{\cos \phi_h}$ structure function

$F_{UU}^{\cos \phi_h}$ structure function is a next-to-leading contribution ($\sim 1/Q$) ⁶. It appears to have many various kinematical and dynamical contributions [2]. We consider contributions from $f_1 D_1$ and $h_1^\perp H_1^\perp$, see Eq. (3.17),

$$F_{UU}^{\cos \phi_h} = \mathcal{C} \left[-\frac{2(\hat{h} \cdot \mathbf{k}_\perp)}{Q} f_1 D_1 \right] + \mathcal{C} \left[-\frac{2\mathbf{k}_\perp^2}{z_h M m_h Q} (\hat{h} \cdot \mathbf{p}_\perp) \kappa h_1^\perp H_1^\perp \right], \quad (4.13)$$

It is the same as in Piloñeta and Vladimirov Ref. [17], compare to Eq. (B.5) in Ref. [17], and in Ebert, Gao, Stewart, Ref. [13], after neglecting “tilde” functions in Eq. (5.41), the same as in Anselmino

⁶The next contribution to $F_{UU}^{\cos \phi_h}$ will be at $1/Q^3$, NNNLP.

et al, Ref. [32], see Eq. (65) of Ref. [32]. This formula coincides with the result of Bacchetta et al, Ref. [2], if one applies EOMs and neglects “tilde” functions in Eq. (4.4), see Appendix B for details.

Historically, $\cos \phi_h$ modulation in SIDIS cross-section was proposed in 70’s by R. Cahn [51] as an argument for the existence of the intrinsic transverse momentum motion of quarks inside of the nucleon, and the first term in Eq. (4.13) as known as Cahn’s term as it originates kinematically from the transverse motion of quarks.

We obtain the following parametrization for $F_{UU}^{\cos \phi_h}$:

$$F_{UU}^{\cos \phi_h}(x, z_h, P_{h\perp}) = -x \sum_a e_a^2 f_1^a(x) D_1^a(z_h) \frac{2\langle k_{\perp}^2 \rangle_{f_1} P_{h\perp} z_h}{Q} \frac{\exp(-P_{h\perp}^2/(z_h^2 \langle k_{\perp}^2 \rangle_{f_1} + \langle p_{\perp}^2 \rangle_{D_1}))}{\pi (z_h^2 \langle k_{\perp}^2 \rangle_{f_1} + \langle p_{\perp}^2 \rangle_{D_1})^2} \\ - x \sum_a e_a^2 h_1^{\perp(1)a}(x) H_1^{\perp(1)a}(z_h) \frac{\lambda_3}{Q} \frac{\exp(-P_{h\perp}^2/(z_h^2 \langle k_{\perp}^2 \rangle_{h_1^{\perp}} + \langle p_{\perp}^2 \rangle_{H_1^{\perp}}))}{\pi (z_h^2 \langle k_{\perp}^2 \rangle_{h_1^{\perp}} + \langle p_{\perp}^2 \rangle_{H_1^{\perp}})^4}, \quad (4.14)$$

where $\lambda_3 = 8Mm_h z_h P_{h\perp} (\langle p_{\perp}^2 \rangle_{H_1^{\perp}}^2 + z_h^2 \langle k_{\perp}^2 \rangle_{h_1^{\perp}} (P_{h\perp}^2 - z_h^2 \langle k_{\perp}^2 \rangle_{h_1^{\perp}}))$.

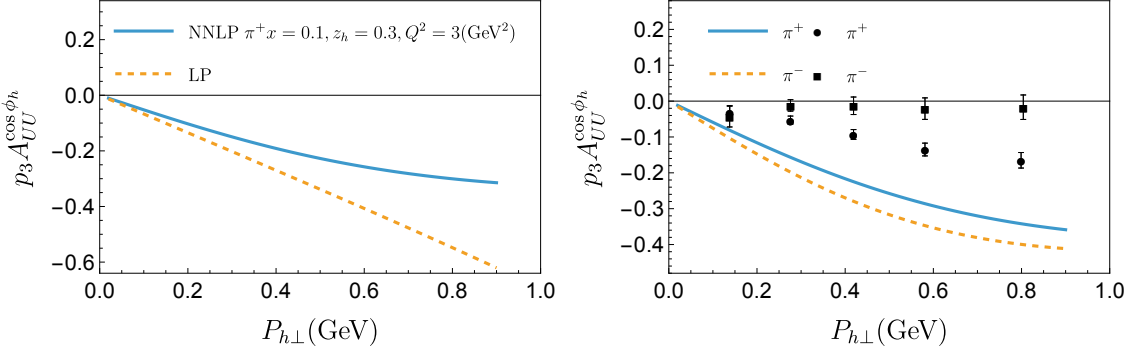


Figure 10: Left panel, $p_3 A_{UU}^{\cos \phi_h}$ for π^+ asymmetry calculated at characteristic HERMES kinematics, $Q^2 = 3 \text{ GeV}^2$, $x = 0.1$, $z_h = 0.3$ r with NNLP terms (blue line) and with LP terms only (orange dashed line) in the denominator. Right panel shows the comparison of our estimates to the HERMES experimental data [52] for π^+ (circles) and π^- (squares).

The asymmetries $A_{UU}^{\cos \phi_h} \sim F_{UU}^{\cos \phi_h} / (F_{UU,T} + p_1 F_{UU,L})$ were measured by EMC [53], Jefferson Lab [54, 55], HERMES [52], and COMPASS [56]. In Fig. 10 we compare our estimates to the HERMES experiment that measured azimuthal asymmetries [52] defined as

$$2\langle \cos \phi_h \rangle \equiv p_3 A_{UU}^{\cos \phi_h} = p_3 \frac{F_{UU}^{\cos \phi_h}}{F_{UU,T} + p_1 F_{UU,L}}. \quad (4.15)$$

In the left panel of Fig. 10 we plot $p_3 A_{UU}^{\cos \phi_h}$ for π^+ production on the hydrogen target at characteristic kinematics of HERMES, $x = 0.1$, $z_h = 0.3$, and $Q^2 = 3 \text{ (GeV}^2)$, using NNLP terms (blue line) and using only leading power terms (dashed orange line) in the denominator of the asymmetry. Right panel of Fig. 10 shows comparison of $p_3 A_{UU}^{\cos \phi_h}$ to the data for π^+ and π^- production. The simple gaussian model that we use has difficulty in describing the data (especially for π^- production), however the description is improved when NLP terms are taken into account.

The COMPASS Collaboration measured $\cos \phi_h$ asymmetries in Ref. [56] defined as

$$A_{\cos \phi_h}^{UU} \equiv A_{UU}^{\cos \phi_h} = \frac{F_{UU}^{\cos \phi_h}}{F_{UU,T} + p_1 F_{UU,L}}, \quad (4.16)$$

and the measurements are performed for h^{\pm} hadrons produced in the scattering of muons at 160 GeV on deuterium target.

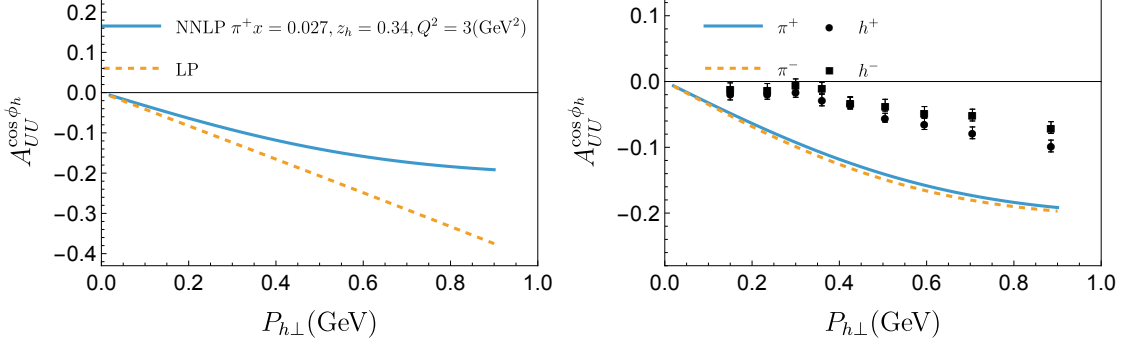


Figure 11: Left panel, $A_{UU}^{\cos\phi_h}$ for π^+ asymmetry calculated at characteristic COMPASS kinematics, $Q^2 = 3 \text{ GeV}^2$, $x = 0.027$, $z_h = 0.34$ with NNLP terms (blue line) and with LP terms only (orange dashed line) in the denominator. Right panel shows the comparison of our estimates for $A_{UU}^{\cos\phi_h}$ to COMPASS experimental data [56] for h^+ (circles) and h^- (squares).

In Fig. 11 we compare our estimates for COMPASS data [56]. Notice that COMPASS collaboration measures h^\pm we approximate charged hadrons as charged pions π^\pm . One can see from Fig. 10 and Fig. 11 that NNLP contributions in the denominator reduce the size of the asymmetry and the asymmetries become closer to the measured ones. It is known that phenomenological description of $\cos\phi_h$ and $\cos 2\phi_h$ modulation is difficult, see i.e. Ref. [40]. It is known that the asymmetry is dominated by the Cahn term (the first term in Eq. (4.13)) and it was shown in Ref. [40] that in a simple parton model $\cos\phi_h$ asymmetries very sensitive to the widths of the distributions and very low values compared to our standard ones were found. In addition, in Ref. [40] the contribution from the Boer-Mulders functions was found to give negligible contribution to the asymmetries. Indeed, one can see from Fig. 10 and Fig. 11 that the predicted difference between π^+ and π^- which are predominantly due to Boer-Mulders contribution (the second term in Eq. (4.13)) and have opposite trends compared to the experimental findings. We believe that a phenomenological analysis that takes into account NLP terms will improve the situation.

4.4 $F_{UU}^{\cos 2\phi_h}$ structure function

$F_{UU}^{\cos 2\phi_h}$ structure function, Eq. (3.18), has leading and next-to-next-to-leading terms

$$F_{UU}^{\cos 2\phi_h} = F_{UU}^{\cos 2\phi_h \text{ LP}} + F_{UU}^{\cos 2\phi_h \text{ NNLP}}, \quad (4.17)$$

$$\begin{aligned} F_{UU}^{\cos 2\phi_h} &= \mathcal{C} \left[\frac{2(\hat{\mathbf{h}} \cdot \mathbf{k}_\perp)(\hat{\mathbf{h}} \cdot \mathbf{p}_\perp) - (\mathbf{k}_\perp \cdot \mathbf{p}_\perp)}{z_h M m_h} \kappa h_1^\perp H_1^\perp \right] \\ &+ \mathcal{C} \left[\frac{2q_T(\hat{\mathbf{h}} \cdot \mathbf{k}_\perp)}{Q^2} f_1 D_1 \right] + \mathcal{C} \left[\frac{2q_T \mathbf{k}_\perp^2}{z_h M m_h Q^2} (\hat{\mathbf{h}} \cdot \mathbf{p}_\perp) \kappa h_1^\perp H_1^\perp \right], \end{aligned} \quad (4.18)$$

where the leading power contribution, the first term in Eq. (4.18) is the same as the standard result, see Ref. [2]. It originates from Boer-Mulders function h_1^\perp convoluted with Collins fragmentation function H_1^\perp . The next-to-next-to-leading power contributions are different from Piloñeta and Vladimirov Ref. [17], compare to Eq. (B.6) in Ref. [17], again due to different results for $\mathcal{S}_0^{\mu\nu} W_{\mu\nu}$ in two formalisms.

In our notations, result from Piloñeta and Vladimirov, Ref. [17], see Eq. (B.6) from Ref. [17], reads

$$F_{UU}^{\cos 2\phi_h} \Big|_{\text{Ref.}[17]} = \mathcal{C} \left[\frac{2(\hat{\mathbf{h}} \cdot \mathbf{k}_\perp)(\hat{\mathbf{h}} \cdot \mathbf{p}_\perp) - (\mathbf{k}_\perp \cdot \mathbf{p}_\perp)}{z_h M m_h} \kappa h_1^\perp H_1^\perp \right]$$

$$\begin{aligned}
& + \mathcal{C} \left[\frac{4(\hat{\mathbf{h}} \cdot \mathbf{k}_\perp)^2}{Q^2} f_1 D_1 \right] - \frac{1}{2} F_{UU,L} \\
& = F_{UU}^{\cos 2\phi_h \text{ LP}} + \frac{4M^2}{Q^2} \mathcal{C} \left[\frac{2(\hat{\mathbf{h}} \cdot \mathbf{k}_\perp)^2 - \mathbf{k}_\perp^2}{2M^2} f_1 D_1 \right] - \mathcal{C} \left[\frac{2\mathbf{k}_\perp^2}{z_h M m_h Q^2} (\mathbf{k}_\perp \cdot \mathbf{p}_\perp) \kappa h_1^\perp H_1^\perp \right]
\end{aligned} \tag{4.19}$$

where leading power term coincides with our calculation, while NNLP terms are different. In particular, contribution to $F_{UU}^{\cos 2\phi_h}$ due to $f_1 D_1$ in Eq. (4.19) coincides with the result from Bachetta et al from Ref [3], see Eq.(6.15) from Ref [3], which was calculated using the generalized parton model of Anselmino et al in Ref. [33]. The contribution in this form is known from the pioneering explorations by R. Cahn in Ref [51], and was used in phenomenology of $\cos 2\phi_h$ asymmetries by Barone, Prokudin, Ma in Ref. [36] and Barone, Melis, Prokudin in Ref. [45]. In the future it will be interesting to investigate $\cos 2\phi_h$ modulations and explore the differences of methodologies of this paper and other frameworks and compare them to the data.

We obtain the following parametrization for $F_{UU}^{\cos 2\phi_h \text{ LP}}$:

$$F_{UU}^{\cos 2\phi_h \text{ LP}}(x, z_h, P_{h\perp}) = x \sum_a e_a^2 h_1^{\perp(1)a}(x) H_1^{\perp(1)a}(z_h) \lambda_4 \frac{\exp(-P_{h\perp}^2/(z_h^2 \langle k_\perp^2 \rangle_{h_1^\perp} + \langle p_\perp^2 \rangle_{H_1^\perp}))}{\pi (z_h^2 \langle k_\perp^2 \rangle_{h_1^\perp} + \langle p_\perp^2 \rangle_{H_1^\perp})^3}, \tag{4.20}$$

where $\lambda_4 = 4M m_h P_{h\perp}^2 z_h^2$, while NNLP contributions will be calculated using Eq. (3.19).

In Fig. 12 we compare our estimates to the HERMES experiment that measured azimuthal asymmetries [52] defined as

$$2\langle \cos 2\phi_h \rangle \equiv p_1 A_{UU}^{\cos 2\phi_h} = p_1 \frac{F_{UU}^{\cos 2\phi_h}}{F_{UU,T} + p_1 F_{UU,L}}. \tag{4.21}$$

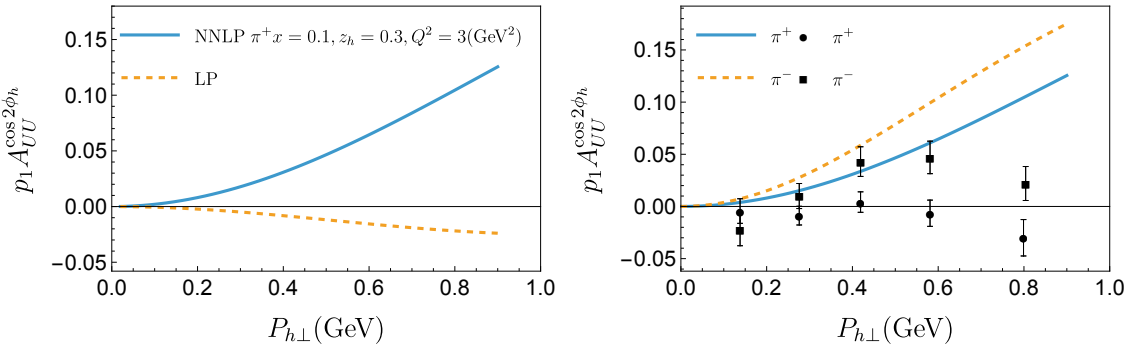


Figure 12: Left panel, $p_1 A_{UU}^{\cos 2\phi_h}$ for π^+ asymmetry calculated at characteristic HERMES kinematics, $Q^2 = 3 \text{ GeV}^2$, $x = 0.1$, $z_h = 0.3$ with NNLP terms (blue line) and with LP terms only (orange dashed line). Right panel shows the comparison of our estimates to HERMES experimental data [52] for π^+ (circles) and π^- (squares).

In the left panel of Fig. 12 we plot $p_1 A_{UU}^{\cos 2\phi_h}$ for π^+ production on the hydrogen target at characteristic kinematics of HERMES, $x = 0.1$, $z_h = 0.3$, and $Q^2 = 3 \text{ (GeV}^2)$, using NLP terms (blue line) and using only leading power terms (dashed orange line) in the denominator of the asymmetry. Right panel of Fig. 12 shows comparison of $p_1 A_{UU}^{\cos 2\phi_h}$ to the data for π^+ and π^- production. Notice that in our formalism, the NLP contributions to $F_{UU}^{\cos 2\phi_h}$ are related to $F_{UU}^{\cos \phi_h}$, see Eq. (3.19). One can see from the left panel of Fig. 12 that the NNLP contributions change

the result drastically. A large contribution from next-to-next-to-leading term in $\cos 2\phi_h$ asymmetry was observed before in Refs. [36, 45].

COMPASS Collaboration measured the asymmetries in Ref. [56] defined as

$$A_{\cos 2\phi_h}^{UU} \equiv A_{UU}^{\cos 2\phi_h} = \frac{F_{UU}^{\cos 2\phi_h}}{F_{UU,T} + p_1 F_{UU,L}}. \quad (4.22)$$

and the measurements are performed for h^\pm hadrons produced in the scattering of muons at 160 GeV on deuterium target. In Fig. 13 we compare our estimates for COMPASS data [56]. Notice that COMPASS collaboration measures h^\pm we approximate charged hadrons as charged pions π^\pm . One can see that the next-to-next-to-leading terms dominate the asymmetry and the trend is opposite to what is observed experimentally.

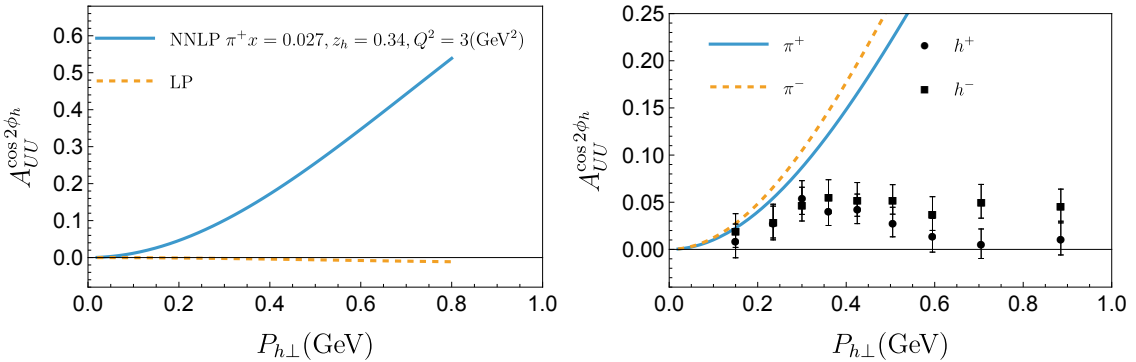


Figure 13: Left panel, $A_{UU}^{\cos 2\phi_h}$ for π^+ asymmetry calculated at characteristic COMPASS kinematics, $Q^2 = 3$ GeV 2 , $x = 0.027$, $z_h = 0.34$ with NNLP terms (blue line) and with LP terms only (orange dashed line). Right panel shows the comparison of our estimates to COMPASS experimental data [56] for h^+ (circles) and h^- (squares) using the full calculation with leading and next-to-next-to-leading contributions.

The Boer-Mulders functions used in our estimates, from Ref [45], were extracted taking into account the next-to-leading Cahn type contribution, see Eq. (B.4). The extraction of Ref [45] had difficulties in describing $P_{h\perp}$ dependent data from HERMES and COMPASS. Similar difficulties were encountered in the analysis of Ref. [40]. Based on our findings we conclude that the leading power Boer-Mulders term to $F_{UU}^{\cos 2\phi_h}$ might not be the leading contribution and a new phenomenological analysis is needed in order to understand better the measured asymmetry. In fact, in the right panel of Fig. 12 one can see that the estimates that include NNLP contributions do not describe the data and have opposite trends compares to the data, i.e. π^- appears to be bigger than π^+ while the data suggests the opposite.

In order to further demonstrate it, we in Fig. 14 plot the leading power terms only:

$$\begin{aligned} p_1 A_{UU}^{\cos 2\phi_h \text{LP}} &= p_1 \frac{F_{UU}^{\cos 2\phi_h \text{LP}}}{F_{UU,T}^{\text{LP}}}, \\ A_{UU}^{\cos 2\phi_h \text{LP}} &= \frac{F_{UU}^{\cos 2\phi_h \text{LP}}}{F_{UU,T}^{\text{LP}}}, \end{aligned} \quad (4.23)$$

for both COMPASS (left panel of Fig. 14) and HERMES (right panel of Fig. 14) experiments. If one assumes the dominance of pions in the charged hadrons, then it is clear that the data are not described by the leading power contributions only, as the leading power contributions are likely to have opposite signs for positive and negative hadrons.

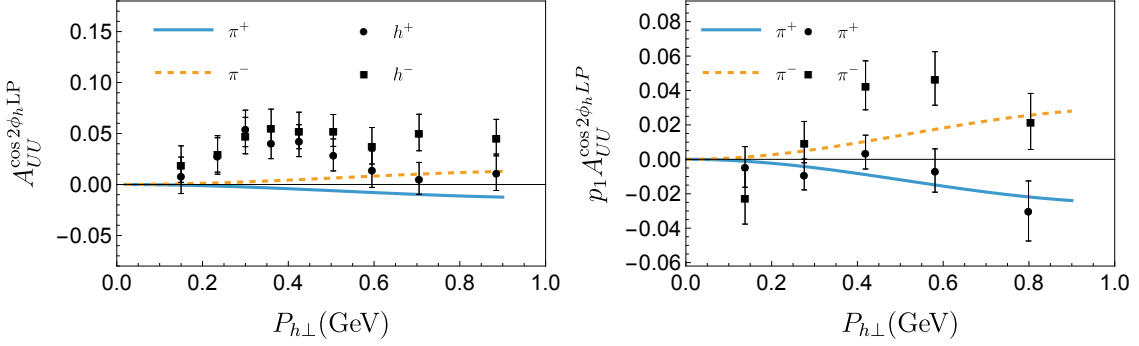


Figure 14: Left panel, $A_{UU}^{\cos 2\phi_h \text{LP}}$ for π^+ asymmetry with leading power terms for π^+ (blue line) and π^- (orange dashed line) compared to COMPASS experimental data [56] for h^+ (circles) and h^- (squares). Right panel, $p_1 A_{UU}^{\cos 2\phi_h}$ asymmetry with only leading power Boer-Mulders contribution for π^+ (blue line) and π^- (orange dashed line) compared to HERMES experimental data [52] for π^+ (circles) and π^- (squares).

4.5 Study of relations Eq. (3.19)

Finally, we would like to address the following question: Can one determine, based on the experimental data, if the proposed relation in Eq. (3.19) between $\cos \phi_h$ and $\cos 2\phi_h$ modulations holds?

It is difficult to address this question using the available experimental data, indeed $F_{UU}^{\cos 2\phi_h}$ has both LP and NNLP contributions. We have seen from Figs. (12,13) that the LP contribution due to Boer-Mulders function convoluted with Collins FF may not be the leading contribution. In addition, Boer-Mulders contribution has opposite sign and approximately same magnitude for π^+ and π^- production, see Fig. 14. We will use this approximate cancellation of Boer-Mulders contribution in the sum of π^+ and π^- and assume that experimental yields of π^+ and π^- are approximately equal. Using the experimental data we will form the sum $A_{UU}^{\cos 2\phi_h \pi^+} + A_{UU}^{\cos 2\phi_h \pi^-}$ which approximately contains only NNLP terms. The same will be done for $F_{UU}^{\cos \phi_h}$, we will form $A_{UU}^{\cos \phi_h \pi^+} + A_{UU}^{\cos \phi_h \pi^-}$ and compare $-q_T/Q(A_{UU}^{\cos \phi_h \pi^+} + A_{UU}^{\cos \phi_h \pi^-})$ to $A_{UU}^{\cos 2\phi_h \pi^+} + A_{UU}^{\cos 2\phi_h \pi^-}$ in Fig. 15.

For the comparison we use the COMPASS data from Ref. [56]. The data is measured for the unidentified charged hadrons, h^\pm , we will assume the dominance of charged pions.

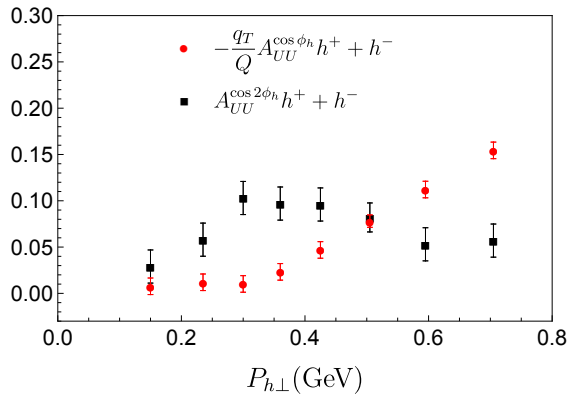


Figure 15: COMPASS experimental data [56] manipulated as described in the text, $-\frac{q_T}{Q}(A_{UU}^{\cos \phi_h h^+} + A_{UU}^{\cos \phi_h h^-})$ red circles, $A_{UU}^{\cos 2\phi_h h^+} + A_{UU}^{\cos 2\phi_h h^-}$ black squares.

If the relation is exact, the red circles should be on top of black squares in Fig. 15. However Fig. 15 demonstrates that the relation of Eq. (3.19) is at most approximate, the sizes and signs of the contributions are similar, however, the shapes are different. Notice that we expect this relation to hold at $1/N_c \sim 30\%$ and $q_T \ll Q$. One also has to be careful interpreting Fig. 15, it is not the result of the experimental measurement, but an estimate that has a lot of assumptions. A more detailed experimental study will be interesting in determining the validity of Eq. (3.19). Based on the available information we conclude that the QCD dynamics is very rich and further theoretical and phenomenological study of our approximations and other terms that we neglected is needed.

5 Conclusions and outlook

In this paper we utilized the rapidity factorization formalism [19] by one of the authors who derived next-to-next-to-leading power ($\sim 1/Q^2$) corrections Ref. [29, 29, 30] to Drell-Yan. We extended calculation to SIDIS process, derived NNLP corrections to the SIDIS hadronic tensor that include convolutions of unpolarized distributions, f_1 , with unpolarized fragmentation, D_1 , functions and Boer-Mulders functions, h_1^\perp , with Collins fragmentation functions, H_1^\perp . We obtained analytic expressions for the unpolarized structure functions in SIDIS, $F_{UU,T}$, $F_{UU,L}$, $F_{UU}^{\cos \phi_h}$, and $F_{UU}^{\cos 2\phi_h}$. $F_{UU,T}$ and $F_{UU}^{\cos 2\phi_h}$ start from leading power and receive NNLP contributions, $F_{UU}^{\cos \phi_h}$ starts from NLP and receives contributions at NNNLP, $1/Q^3$; while $F_{UU,L}$ starts from NNLP. We presented our results in both momentum and coordinate spaces making our formulas useful for phenomenology.

Using a simple model for TMD PDFs and TMD FFs we provided numerical estimates and compared our results to the data from HERMES and COMPASS experiments. We also provided predictions to the future measurements of R_{SIDIS} at Jefferson Lab and the future Electron-Ion Collider. We compared our formulas to the existing literature and found mostly agreement of various formalisms, however some differences exist and the future theoretical phenomenological studies will be important to verify our relationships and to study the differences. The size of the next-to-leading and next-to-next-to-leading power corrections warrants their usage in phenomenology, especially for the data at low Q^2 . In this regard Jefferson Lab and the future EIC data will have to be explored taking into account NLP and NNLP corrections.

In the future we are planning to study the polarized structure functions in SIDIS and to explore NNLP corrections from other terms in the hadronic tensor that we did not consider in this publication. We also plan on implementing NLP and NNLP corrections in phenomenology with full TMD evolution.

Acknowledgments

We would like to thank Iain Stewart for correspondence and stimulating discussions, Leonard Gamberg and Alexey Vladimirov for discussions and comments on the manuscript. This work was supported by the U.S. Department of Energy contract No. DE-AC05-06OR23177, under which Jefferson Science Associates, LLC operates Jefferson Lab (I.B.,A.P.), and within the framework of the Saturated Glue (SURGE) Topical Theory Collaboration (I.B.), and by the U.S. Department of Energy grant No. DE-FG02-97ER41028 (I.B.), and by the National Science Foundation under Grants No. PHY-2310031, No. PHY-2335114 (A.P.). The research reported here is connected with the Quark-Gluon Tomography Collaboration supported by the U.S. Department of Energy, Office of Science, Office of Nuclear Physics under contract DE-SC0023646 (A.P.).

A Conversions

There exist several different notations for the vectors in hadron-hadron and in photon-hadron frames. In order to facilitate the comparison of the results we will list the papers we investigate in our publication and comment on the notations.

- Pilõneta and Vladimirov in Ref. [17] explore both frames and provide final results in hadron-hadron frame. Transverse vectors in photon-hadron frame are denoted by \perp while those in hadron-hadron frame are denoted by \mathbf{T} . The vectors in Eqs. (B.3-B.6) of Ref. [17] are related to our notations as follows:

$$[\mathbf{k}_1]_{\text{Ref.}[17]} = [\mathbf{k}_\perp]_{\text{our}} , \quad (\text{A.1})$$

$$[\mathbf{k}_2]_{\text{Ref.}[17]} = \left[-\frac{\mathbf{p}_\perp}{z_h} \right]_{\text{our}} , \quad (\text{A.2})$$

$$[\mathbf{h}_T]_{\text{Ref.}[17]} = \left[-\hat{\mathbf{h}} \right]_{\text{our}} . \quad (\text{A.3})$$

- Ebert, Gao, and Stewart in Ref. [13] work in hadron-hadron frame. They parametrize $\mathbf{q}_T = q_T(-1, 0)$ and thus $\hat{\mathbf{h}} = (1, 0)$. In order to compare their notations for the convolutions we use

$$[k_{Tx}]_{\text{Ref.}[13]} = \left[\hat{\mathbf{h}} \cdot \mathbf{k}_T \right]_{\text{our}} = \left[\hat{\mathbf{h}} \cdot \mathbf{k}_\perp \right]_{\text{our}} , \quad (\text{A.4})$$

$$[p_{Tx}]_{\text{Ref.}[13]} = \left[\hat{\mathbf{h}} \cdot \mathbf{p}'_T \right]_{\text{our}} = \left[-\frac{\hat{\mathbf{h}} \cdot \mathbf{p}_\perp}{z_h} \right]_{\text{our}} , \quad (\text{A.5})$$

- Bacchetta et al in Ref. [2] work in hadron-hadron frame. The conversion of vectors read

$$[\mathbf{p}_T]_{\text{Ref.}[2]} = [\mathbf{k}_\perp]_{\text{our}} , \quad (\text{A.6})$$

$$[\mathbf{k}_T]_{\text{Ref.}[2]} = \left[-\frac{\mathbf{p}_\perp}{z_h} \right]_{\text{our}} , \quad (\text{A.7})$$

$$\left[\hat{\mathbf{h}} \right]_{\text{Ref.}[2]} = \left[\hat{\mathbf{h}} \right]_{\text{our}} . \quad (\text{A.8})$$

Notice that in the convolution of Eq. (4.1) of Ref. [2] one should use $D^a(z, \mathbf{k}_T^2) \rightarrow D^a(z, z^2 \mathbf{k}_T^2)$.

- Anselmino et al in Ref. [32] work in photon-hadron frame. The conversion of vectors read

$$[\mathbf{k}_\perp]_{\text{Ref.}[32]} = [\mathbf{k}_\perp]_{\text{our}} , \quad (\text{A.9})$$

$$[\mathbf{p}_\perp]_{\text{Ref.}[32]} = \left[-\frac{\mathbf{p}_\perp}{z_h} \right]_{\text{our}} , \quad (\text{A.10})$$

$$[\mathbf{P}_T]_{\text{Ref.}[32]} = [\mathbf{P}_{h\perp}]_{\text{our}} , \quad (\text{A.11})$$

$$\left[\hat{\mathbf{P}}_T \right]_{\text{Ref.}[32]} = \left[\hat{\mathbf{h}} \right]_{\text{our}} . \quad (\text{A.12})$$

B Structure functions from Refs. [1–3]

For completeness, in this Appendix we will report the structure functions given by [1–3] using our notations ⁷

$$F_{UU,T} = \mathcal{C}[f_1 D_1] , \quad (\text{B.1})$$

⁷In these formulas h_1^\perp is for SIDIS.

$$F_{UU,L} = \frac{4M^2}{Q^2} \mathcal{C} \left[\frac{\mathbf{k}_\perp^2}{M^2} f_1 D_1 \right], \quad (\text{B.2})$$

$$F_{UU}^{\cos \phi_h} = \frac{2M_N}{Q} \mathcal{C} \left[\frac{\hat{\mathbf{h}} \cdot \mathbf{p}_\perp}{zm_h} \left(xh H_1^\perp + \frac{m_h}{M} f_1 \frac{\tilde{D}^\perp}{z} \right) - \frac{\hat{\mathbf{h}} \cdot \mathbf{k}_\perp}{M_N} \left(xf^\perp D_1 + \frac{m_h}{M_N} h_1^\perp \frac{\tilde{H}}{z} \right) \right], \quad (\text{B.3})$$

$$F_{UU}^{\cos 2\phi_h} = \mathcal{C} \left[\frac{2(\hat{\mathbf{h}} \cdot \mathbf{k}_\perp)(\hat{\mathbf{h}} \cdot \mathbf{p}_\perp) - \mathbf{k}_\perp \cdot \mathbf{p}_\perp}{zMm_h} h_1^\perp H_1^\perp \right] + \frac{4M^2}{Q^2} \mathcal{C} \left[\frac{2(\hat{\mathbf{h}} \cdot \mathbf{k}_\perp)^2 - \mathbf{k}_\perp^2}{2M^2} f_1 D_1 \right]. \quad (\text{B.4})$$

The equation of motion relations arise if one works in the tree level of hard interactions, see Ref. [9], and in the chiral even sector [1, 2, 57] the equations read

$$xf^\perp = x\tilde{f}^\perp + f_1, \quad xh = x\tilde{h} + \frac{k_\perp^2}{M^2} h_1^\perp, \quad (\text{B.5})$$

$$\frac{D^\perp}{z} = \frac{\tilde{D}^\perp}{z} + D_1, \quad \frac{H}{z} = \frac{\tilde{H}}{z} + \frac{p_\perp^2}{z^2 M_h^2} H_1^\perp. \quad (\text{B.6})$$

Note that $k_\perp^2 = -\mathbf{k}_\perp^2$ and $p_\perp^2 = -\mathbf{p}_\perp^2$. If one applies the Wandzura-Wilczek approximation, i.e. sets all dynamical functions labeled with a tilde to zero, then $F_{UU}^{\cos \phi_h}$ in Eq. (B.3), becomes, see e.g. Ref. [9]:

$$F_{UU}^{\cos \phi_h} = \frac{2M}{Q} \mathcal{C} \left[-\frac{\hat{\mathbf{h}} \cdot \mathbf{p}_\perp}{zm_h} \frac{\mathbf{k}_\perp^2}{M} h_1^\perp H_1^\perp - \frac{\hat{\mathbf{h}} \cdot \mathbf{k}_\perp}{M} f_1 D_1 \right], \quad (\text{B.7})$$

and one can see that we reproduce our Eq. (4.13). The next-to-leading power (NLP) terms present in $F_{UU,L}$, Eq. (4.8), and in the second term of $F_{UU}^{\cos 2\phi_h}$, Eq. (4.18), are derived in Bachetta et al Ref. [3] using parton model calculation of Anselmino et al, Ref. [33]. The second term in Eq. (B.7) and Eq. (4.18) is referred to as Cahn effect, Refs. [51, 58].

One can also express convolutions in Eq. (B.1), (B.2), (B.7), and (B.4) through Fourier transforms of products of TMDs in b_T space [31],

$$F_{UU,T} = \mathcal{B} \left[\tilde{f}_1^{(0)} \tilde{D}_1^{(0)} \right], \quad (\text{B.8})$$

$$F_{UU,L} = \frac{4}{Q^2} \mathcal{B} \left[\widetilde{k_\perp^2 f_1}^{(0)} \tilde{D}_1^{(0)} \right], \quad (\text{B.9})$$

$$F_{UU}^{\cos \phi_h} = -\frac{2M^2}{Q} \mathcal{B} \left[\tilde{f}_1^{(1)} \tilde{D}_1^{(0)} \right] - \frac{2m_h}{QM} \mathcal{B} \left[\widetilde{k_\perp^2 h_1^\perp}^{(0)} \tilde{H}_1^{\perp(1)} \right], \quad (\text{B.10})$$

$$F_{UU}^{\cos 2\phi_h} = M m_h \mathcal{B} \left[\tilde{h}_1^{\perp(1)} \tilde{H}_1^{\perp(1)} \right] + \frac{M^4}{Q^2} \mathcal{B} \left[\tilde{f}_1^{(2)} \tilde{D}_1^{(0)} \right]. \quad (\text{B.11})$$

References

- [1] P.J. Mulders and R.D. Tangerman, *The Complete tree level result up to order $1/Q$ for polarized deep inelastic lepto production*, *Nucl. Phys. B* **461** (1996) 197 [[hep-ph/9510301](#)].
- [2] A. Bacchetta, M. Diehl, K. Goeke, A. Metz, P.J. Mulders and M. Schlegel, *Semi-inclusive deep inelastic scattering at small transverse momentum*, *JHEP* **02** (2007) 093 [[hep-ph/0611265](#)].
- [3] A. Bacchetta, D. Boer, M. Diehl and P.J. Mulders, *Matches and mismatches in the descriptions of semi-inclusive processes at low and high transverse momentum*, *JHEP* **08** (2008) 023 [[0803.0227](#)].
- [4] HERMES collaboration, *The HERMES polarized hydrogen and deuterium gas target in the HERA electron storage ring*, *Nucl. Instrum. Meth. A* **540** (2005) 68 [[physics/0408137](#)].

[5] COMPASS collaboration, *The COMPASS experiment at CERN*, *Nucl. Instrum. Meth. A* **577** (2007) 455 [[hep-ex/0703049](#)].

[6] J. Dudek et al., *Physics Opportunities with the 12 GeV Upgrade at Jefferson Lab*, *Eur. Phys. J. A* **48** (2012) 187 [[1208.1244](#)].

[7] R. Abdul Khalek et al., *Science Requirements and Detector Concepts for the Electron-Ion Collider: EIC Yellow Report*, *Nucl. Phys. A* **1026** (2022) 122447 [[2103.05419](#)].

[8] J. Collins, *Foundations of perturbative QCD*, vol. 32, Cambridge University Press (11, 2013).

[9] R. Boussarie et al., *TMD Handbook*, [2304.03302](#).

[10] A. Kotzinian, *New quark distributions and semiinclusive electroproduction on the polarized nucleons*, *Nucl. Phys. B* **441** (1995) 234 [[hep-ph/9412283](#)].

[11] HALL C SIDIS collaboration, *Flavor, transverse momentum, and azimuthal dependence of charged pion multiplicities in SIDIS with 10.6 GeV electrons*, [2510.03562](#).

[12] J.P. Ralston and D.E. Soper, *Production of Dimuons from High-Energy Polarized Proton Proton Collisions*, *Nucl. Phys. B* **152** (1979) 109.

[13] M.A. Ebert, A. Gao and I.W. Stewart, *Factorization for azimuthal asymmetries in SIDIS at next-to-leading power*, *JHEP* **06** (2022) 007 [[2112.07680](#)].

[14] S. Rodini and A. Vladimirov, *Transverse momentum dependent factorization for SIDIS at next-to-leading power*, *Phys. Rev. D* **110** (2024) 034009 [[2306.09495](#)].

[15] A. Vladimirov, V. Moos and I. Scimemi, *Transverse momentum dependent operator expansion at next-to-leading power*, *JHEP* **01** (2022) 110 [[2109.09771](#)].

[16] A. Vladimirov, *Kinematic power corrections in TMD factorization theorem*, *JHEP* **12** (2023) 008 [[2307.13054](#)].

[17] S. Piloneta and A. Vladimirov, *Kinematic power corrections for TMD factorization theorem of semi-inclusive deep-inelastic scattering*, [2510.14496](#).

[18] M. Jaarsma, O. del Rio, I. Scimemi and W. Waalewijn, *Soft background fields at next-to-leading power in transverse momentum dependent SIDIS with jets*, *JHEP* **11** (2025) 014 [[2507.03072](#)].

[19] I. Balitsky and A. Tarasov, *Higher-twist corrections to gluon TMD factorization*, *JHEP* **07** (2017) 095 [[1706.01415](#)].

[20] I. Balitsky, *Gauge-invariant TMD factorization for Drell-Yan hadronic tensor at small x* , *JHEP* **05** (2021) 046 [[2012.01588](#)].

[21] I. Balitsky, *$1/Q^2$ power corrections to TMD factorization for Drell-Yan hadronic tensor*, *Nucl. Phys. B* **1006** (2024) 116658 [[2404.15116](#)].

[22] D. Boer and P.J. Mulders, *Time reversal odd distribution functions in lepton production*, *Phys. Rev. D* **57** (1998) 5780 [[hep-ph/9711485](#)].

[23] J.C. Collins, *Fragmentation of transversely polarized quarks probed in transverse momentum distributions*, *Nucl. Phys. B* **396** (1993) 161 [[hep-ph/9208213](#)].

[24] A. Bacchetta, U. D'Alesio, M. Diehl and C.A. Miller, *Single-spin asymmetries: The Trento conventions*, *Phys. Rev. D* **70** (2004) 117504 [[hep-ph/0410050](#)].

[25] S. Bastami et al., *Semi-Inclusive Deep Inelastic Scattering in Wandzura-Wilczek-type approximation*, *JHEP* **06** (2019) 007 [[1807.10606](#)].

[26] D. Boer, P.J. Mulders and F. Pijlman, *Universality of T odd effects in single spin and azimuthal asymmetries*, *Nucl. Phys. B* **667** (2003) 201 [[hep-ph/0303034](#)].

[27] S. Meissner, A. Metz and D. Pitonyak, *Momentum sum rules for fragmentation functions*, *Phys. Lett. B* **690** (2010) 296 [[1002.4393](#)].

[28] A. Metz and A. Vossen, *Parton Fragmentation Functions*, *Prog. Part. Nucl. Phys.* **91** (2016) 136 [[1607.02521](#)].

[29] I. Balitsky, *Drell-Yan angular lepton distributions at small x from TMD factorization.*, *JHEP* **09** (2021) 022 [[2105.13391](#)].

[30] I. Balitsky and A. Tarasov, *Power corrections to TMD factorization for Z-boson production*, *JHEP* **05** (2018) 150 [[1712.09389](#)].

[31] D. Boer, L. Gamberg, B. Musch and A. Prokudin, *Bessel-Weighted Asymmetries in Semi Inclusive Deep Inelastic Scattering*, *JHEP* **10** (2011) 021 [[1107.5294](#)].

[32] M. Anselmino, M. Boglione, U. D'Alesio, S. Melis, F. Murgia, E.R. Nocera et al., *General Helicity Formalism for Polarized Semi-Inclusive Deep Inelastic Scattering*, *Phys. Rev. D* **83** (2011) 114019 [[1101.1011](#)].

[33] M. Anselmino, M. Boglione, U. D'Alesio, A. Kotzinian, F. Murgia and A. Prokudin, *The Role of Cahn and sivers effects in deep inelastic scattering*, *Phys. Rev. D* **71** (2005) 074006 [[hep-ph/0501196](#)].

[34] J.C. Collins, A.V. Efremov, K. Goeke, S. Menzel, A. Metz and P. Schweitzer, *Sivers effect in semi-inclusive deeply inelastic scattering*, *Phys. Rev. D* **73** (2006) 014021 [[hep-ph/0509076](#)].

[35] U. D'Alesio and F. Murgia, *Azimuthal and Single Spin Asymmetries in Hard Scattering Processes*, *Prog. Part. Nucl. Phys.* **61** (2008) 394 [[0712.4328](#)].

[36] V. Barone, A. Prokudin and B.-Q. Ma, *A Systematic phenomenological study of the $\cos 2 \phi$ asymmetry in unpolarized semi-inclusive DIS*, *Phys. Rev. D* **78** (2008) 045022 [[0804.3024](#)].

[37] P. Schweitzer, T. Teckentrup and A. Metz, *Intrinsic transverse parton momenta in deeply inelastic reactions*, *Phys. Rev. D* **81** (2010) 094019 [[1003.2190](#)].

[38] A. Signori, A. Bacchetta, M. Radici and G. Schnell, *Investigations into the flavor dependence of partonic transverse momentum*, *JHEP* **11** (2013) 194 [[1309.3507](#)].

[39] M. Anselmino, M. Boglione, J.O. Gonzalez Hernandez, S. Melis and A. Prokudin, *Unpolarised Transverse Momentum Dependent Distribution and Fragmentation Functions from SIDIS Multiplicities*, *JHEP* **04** (2014) 005 [[1312.6261](#)].

[40] V. Barone, M. Boglione, J.O. Gonzalez Hernandez and S. Melis, *Phenomenological analysis of azimuthal asymmetries in unpolarized semi-inclusive deep inelastic scattering*, *Phys. Rev. D* **91** (2015) 074019 [[1502.04214](#)].

[41] JEFFERSON LAB ANGULAR MOMENTUM collaboration, *Origin of single transverse-spin asymmetries in high-energy collisions*, *Phys. Rev. D* **102** (2020) 054002 [[2002.08384](#)].

[42] JEFFERSON LAB ANGULAR MOMENTUM (JAM), JEFFERSON LAB ANGULAR MOMENTUM collaboration, *Updated QCD global analysis of single transverse-spin asymmetries: Extracting H^\sim , and the role of the Soffer bound and lattice QCD*, *Phys. Rev. D* **106** (2022) 034014 [[2205.00999](#)].

[43] A.D. Martin, W.J. Stirling, R.S. Thorne and G. Watt, *Parton distributions for the LHC*, *Eur. Phys. J. C* **63** (2009) 189 [[0901.0002](#)].

[44] D. de Florian, R. Sassot and M. Stratmann, *Global analysis of fragmentation functions for pions and kaons and their uncertainties*, *Phys. Rev. D* **75** (2007) 114010 [[hep-ph/0703242](#)].

[45] V. Barone, S. Melis and A. Prokudin, *The Boer-Mulders effect in unpolarized SIDIS: An Analysis of the COMPASS and HERMES data on the $\cos 2 \phi$ asymmetry*, *Phys. Rev. D* **81** (2010) 114026 [[0912.5194](#)].

[46] M. Anselmino, M. Boglione, U. D'Alesio, S. Melis, F. Murgia and A. Prokudin, *Simultaneous extraction of transversity and Collins functions from new SIDIS and e+e- data*, *Phys. Rev. D* **87** (2013) 094019 [[1303.3822](#)].

[47] A. Accardi et al., *Strong interaction physics at the luminosity frontier with 22 GeV electrons at Jefferson Lab*, *Eur. Phys. J. A* **60** (2024) 173 [[2306.09360](#)].

[48] HERMES collaboration, *Multiplicities of charged pions and kaons from semi-inclusive deep-inelastic scattering by the proton and the deuteron*, *Phys. Rev. D* **87** (2013) 074029 [[1212.5407](#)].

[49] MAP (MULTI-DIMENSIONAL ANALYSES OF PARTONIC DISTRIBUTIONS) collaboration, *Unpolarized transverse momentum distributions from a global fit of Drell-Yan and semi-inclusive deep-inelastic scattering data*, *JHEP* **10** (2022) 127 [[2206.07598](#)].

[50] COMPASS collaboration, *Transverse-momentum-dependent Multiplicities of Charged Hadrons in Muon-Deuteron Deep Inelastic Scattering*, *Phys. Rev. D* **97** (2018) 032006 [[1709.07374](#)].

[51] R.N. Cahn, *Azimuthal Dependence in Leptoproduction: A Simple Parton Model Calculation*, *Phys. Lett. B* **78** (1978) 269.

[52] HERMES collaboration, *Azimuthal distributions of charged hadrons, pions, and kaons produced in deep-inelastic scattering off unpolarized protons and deuterons*, *Phys. Rev. D* **87** (2013) 012010 [[1204.4161](#)].

[53] EUROPEAN MUON collaboration, *Measurement of Hadronic Azimuthal Distributions in Deep Inelastic Muon Proton Scattering*, *Phys. Lett. B* **130** (1983) 118.

[54] CLAS collaboration, *Measurement of unpolarized semi-inclusive π^+ electroproduction off the proton*, *Phys. Rev. D* **80** (2009) 032004 [[0809.1153](#)].

[55] H. Mkrtchyan et al., *Transverse momentum dependence of semi-inclusive pion production*, *Phys. Lett. B* **665** (2008) 20 [[0709.3020](#)].

[56] COMPASS collaboration, *Measurement of azimuthal hadron asymmetries in semi-inclusive deep inelastic scattering off unpolarised nucleons*, *Nucl. Phys. B* **886** (2014) 1046 [[1401.6284](#)].

[57] R.D. Tangerman and P.J. Mulders, *Polarized twist - three distributions $g(T)$ and $h(L)$ and the role of intrinsic transverse momentum*, [hep-ph/9408305](#).

[58] R.N. Cahn, *Critique of Parton Model Calculations of Azimuthal Dependence in Leptoproduction*, *Phys. Rev. D* **40** (1989) 3107.